AFRRI CR67-1
RRA-T71
FEBRUARY 1967

AFRRI CONTRACT REPORT

AFRRI CR67-1
RRA-T71

AD658043

CALCULATED GAMMA-RAY DOSE DISTRIBUTIONS IN A PHANTOM EXPOSED TO FALLOUT AND SIMULATED FALLOUT

R.L. French, RRA
K.W. Tompkins, RRA
C.W. Garrett, AFRRI

Prepared Under Contract by
RADIATION RESEARCH ASSOCIATES, INC.
Fort Worth, Texas
for
ARMED FORCES RADIOBIOLOGY RESEARCH INSTITUTE
Defense Atomic Support Agency
Bethesda, Maryland

15

Distribution of this document is unlimited

AFRRI CR67-1
RRA-T71
February 1967

CALCULATED GAMMA-RAY DOSE DISTRIBUTIONS IN A PHANTOM EXPOSED TO FALLOUT AND SIMULATED FALLOUT

R. L. FRENCH, RRA
K. W. TOMPKINS, RRA
C. W. GARRETT, AFRRI

Report Prepared by
RADIATION RESEARCH ASSOCIATES, INC.
Fort Worth, Texas
Under Contract No. DA-49-146-XZ-479

J S Burkle
J. S. BURKLE
Captain, MC, USN
Director

ARMED FORCES RADIOBIOLOGY RESEARCH INSTITUTE
Defense Atomic Support Agency
Bethesda, Maryland

ACKNOWLEDGMENTS

The authors are grateful to J. H. Price who made special modifications to the COHORT Monte Carlo code to accommodate the depth-dose problems, to D. G. Collins for many helpful discussions on the utilization of COHORT, and to L. Olmedo for his assistance with the analytic calculations. A special acknowledgment is due Dr. James T. Brennan, formerly Director of the Armed Forces Radiobiology Research Institute and currently the Mathew J. Wilson Professor in Research Radiology at the University of Pennsylvania, for suggesting the investigation.

ABSTRACT

Gamma-ray depth-dose distributions in a phantom exposed to fallout and to simulated fallout were calculated by the Monte Carlo method. The phantom consisted of a tissue equivalent vertical right cylinder of 60 cm height and 30 cm in diameter. The center of the phantom was 3 ft 8 in.(111.8 cm) above a smooth ground surface uniformly contaminated with ^{235}U fission products. The energy and angle distribution of the gamma rays incident upon the phantom were taken from previous Monte Carlo calculations.

The depth-dose distributions were found to be relatively insensitive to fallout age over the period investigated (1 hour to 9 days). The dose rate at the center of the phantom is approximately 65 percent of the free-field dose rate, while that at the lateral surface is approximately 80 percent. Except near the extremities, the dose rate along the vertical axis of the phantom varies at approximately the same rate with height above ground as does the free-field dose rate. Approximately one-half of the dose rate at the center of the phantom is from photons which have suffered previous collisions in the phantom.

The depth-dose distributions were calculated for two arrangements of artificial sources which, although not duplicating the fallout energy spectra, were intended to produce similar depth-dose distributions. The patterns produced by revolving the phantom on its vertical axis while exposed to a point ^{60}Co source at a horizontal distance of 200 ft (61 m) are similar to those from the fallout, except for internal positions near the bottom of the phantom. A special arrangement of ^{60}Co, ^{137}Cs and ^{144}Ce sources produced substantially the same depth-dose patterns throughout the phantom as did the fallout.

An additional calculation was performed of the depth-dose distribution within a phantom positioned at the center of a 4 ft diameter by 5 ft deep foxhole located in a 1.12-hr fallout field. The distribution in the horizontal midplane of the phantom was found to be quite similar in shape to the above ground case except for a sharper dropoff of the dose away from the lateral surface. As would be expected, however, the axial distribution is quite different from that found above ground.

TABLE OF CONTENTS

LIST OF FIGURES

LIST OF TABLES

BLANK PAGE

I. INTRODUCTION

The Armed Forces Radiobiology Research Institute (AFRRI) has been engaged in a continuing study of the radiation fields associated with fallout and laboratory irradiation devices (fallout simulators) which could be used to study the biological effects of exposure to fallout. This report describes a recently-completed phase of this effort in which depth-dose distributions in cylindrical phantoms were computed for several relevant geometries: (1) above idealized fallout fields of several ages, (2) in two different fallout simulators, and (3) in a foxhole placed in a fallout field.

Investigations of the physical nature of fallout fields have been underway for many years. Both experimental and theoretical techniques have been employed. During the era of atmospheric nuclear testing, several studies of actual fallout fields were conducted.[1,2,3*] Artificial fallout fields have been temporarily constructed using isotope sources,[4,5,6,7,8*] more permanent laboratory irradiation devices have been used as fallout simulators[9,10,11*] and others have been proposed.[12,13*] Whereas there is much in the literature on the free-field properties of gamma rays from fallout and fallout simulators, (Spencer's[14] work being a notable example) there is very little that is concerned with depth-dose data. Imirie and Sharp[15] measured some depth-dose and absorption profiles in masonite man phantoms placed in an actual fallout field to determine the relative contribution of beta and gamma radiations. Bond et al.[16] reviewed depth-dose patterns obtained experimentally for several source geometries including fallout and clearly showed the importance of understanding depth-dose distributions.

Although this early work served to define the problem, the techniques employed were not very precise when compared to present

---

* - The references quoted are illustrative and do not exhaust the available literature.

day standards. Further, no definitive calculations of fallout-related depth-dose distributions have been reported. The study reported herein was performed by Radiation Research Associates, Inc. (RRA) under contract to and in collaboration with the AFRRI, and consisted of using Monte Carlo techniques to compute the gamma-ray depth-dose patterns in tissue-equivalent homogeneous phantoms placed at appropriate locations in the geometries considered. Beta rays from fallout which cannot penetrate as deeply into the body as can gamma rays were not considered in the present study.

Earlier studies[17,18] characterized the gamma-ray fields at selected point receiver positions in the geometries of interest by describing the photon angle and energy distributions of the free fields from which the dose* in tissue was obtained. (The "free field" is a radiation field existing in unshielded or shielded regions without the field-perturbing biological specimen present.) These earlier results, which are summarized in Chapter II, were used as source data to compute the depth-dose distributions along the central (vertical) axis and along a midplane diameter of a phantom placed at the point receiver positions.

A Monte Carlo approach was selected for performing the depth-dose calculations because it allows a more accurate treatment of the radiation environment and of the finite size and geometry of the phantom than do analytic methods for solving the radiation transport problem. However, to provide guidance for the Monte Carlo calculations and to determine the degree of validity of a

* - Actually, the kerma in tissue was the quantity computed in the earlier studies and in the present study. As charged particle equilibrium in a low-z material is closely approximated for all free-field positions, the numerical values of the kerma in tissue and the absorbed dose in a small piece of tissue are nearly identical. To be consistent with the terminology of the referenced works, we shall use the term "dose" throughout this report.

simpler method, calculations were also performed using exponential attenuation and infinite medium dose buildup factors. Chapter III describes the methods used in the depth-dose calculations.

The results of the depth-dose calculations, given in Chapter IV, are expressed as the fraction of the free-field dose rate in tissue at the point receiver position over which the phantom was superimposed. Obtained as intermediate and auxiliary results were the differential energy spectrum of the flux density at a number of positions in the phantom and the fraction of the total incident energy which is absorbed in the phantom. The various results were compared and analyzed to determine their sensitivity to fallout age, to determine the extent to which the fallout simulators do simulate fallout depth-dose distributions, and to establish the validity of the calculational methods.

Some conclusions concerning the results obtained and the validity of the computational methods used are given in the final chapter of this report. The appendix contains a tabulation of the radiation environment data used as input to the depth-dose calculations.

II. RADIATION ENVIRONMENTS

To calculate the transport of photons in the phantom, it was first necessary to obtain the energy and angle distributions of the photons incident upon the phantom. The results of earlier Monte Carlo calculations,[17,18] in which the free-field angle and energy distribution of the number flux density was determined at point receivers for the geometries under investigation, were used for this purpose.

The idealized fallout radiation environments were determined for a receiver located 3 ft (0.914 m) above fallout uniformly deposited on a smooth ground surface.[17] The fallout was assumed to consist of non-volatile ^{235}U fission products; fallout ages of 1.12 hours, 23.8 hours, 4.57 days and 9.82 days were separately examined.

One of the two simulated fallout radiation environments studied was that produced by a point isotropic ^{60}Co source (~1.25 MeV) elevated 3 ft above the ground and placed 200 ft (61 m) horizontally from a similarly elevated receiver. The other was that produced by a special arrangement of ^{60}Co, ^{137}Cs (~0.67 MeV) and ^{144}Ce (~0.10 MeV) sources known as the AFRRI Compact Simulator.[18]

The radiation environment in a 5 ft deep by 4 ft diameter foxhole dug in a fallout field was also based on earlier calculations,[18] but it was necessary to make a correction to a minor component and extend the calculations to additional positions in the foxhole (see Sec. 2.3). This section summarizes these free-field calculations which are more fully described in the earlier reports.[17,18]

2.1 Fallout

For the fallout fields the basic computations were of the energy and angle distribution of the photon flux density above infinite plane isotropic sources of monoenergetic gamma rays with energies of 0.10, 0.14, 0.25, 0.40, 0.67, 0.85, 1.25, 1.75, 2.50 and 3.50 MeV. The results of these individual calculations were weighted by the ^{235}U fission product decay spectra of Nelms and Cooper[19] and then combined to obtain data for fallout of several different ages.

Figure 1A shows the geometry used in the fallout calculations. Also shown in Figure 1A for illustrative purposes is the phantom superimposed over the receiver point. For each source the uncollided and scattered flux densities at the receiver point were computed in each of ten energy intervals between 0.04 and 3.5 MeV and eighteen equal receiver polar angle (θ) intervals between 0° and 180°. In addition to the flux densities, the dose rate arriving through each ten-degree interval of receiver angle was computed. All results were integrated over azimuthal angle (ϕ) to provide distributions as a function of polar angle only.

For calculations of the uncollided components, exponential and inverse square attenuation were considered and an air composition of 22 percent (number density) oxygen and 78 percent nitrogen was assumed. Grodstein's gamma-ray cross sections[20] and an air density of 1.29×10^{-3} g/cm^3 were used. The calculations required an integration of the attenuation kernel over the surface of the infinite plane source. The receiver polar angle (θ) was selected as the variable of integration and, using a machine program, an increment $\Delta\theta$ of one minute was used in integrating over each ten-degree interval of receiver angle.

The air- and ground-scattered flux densities were computed with the L05 Monte Carlo Program.[21] In these calculations a ground composition corresponding to Nevada Test Site soil was used. The L05 program allowed essentially exact representation of the air/ground geometry and composition. The infinite plane source, which could not be treated directly by the program, was approximated by a set of 23 point isotropic sources, each of which represented an annular

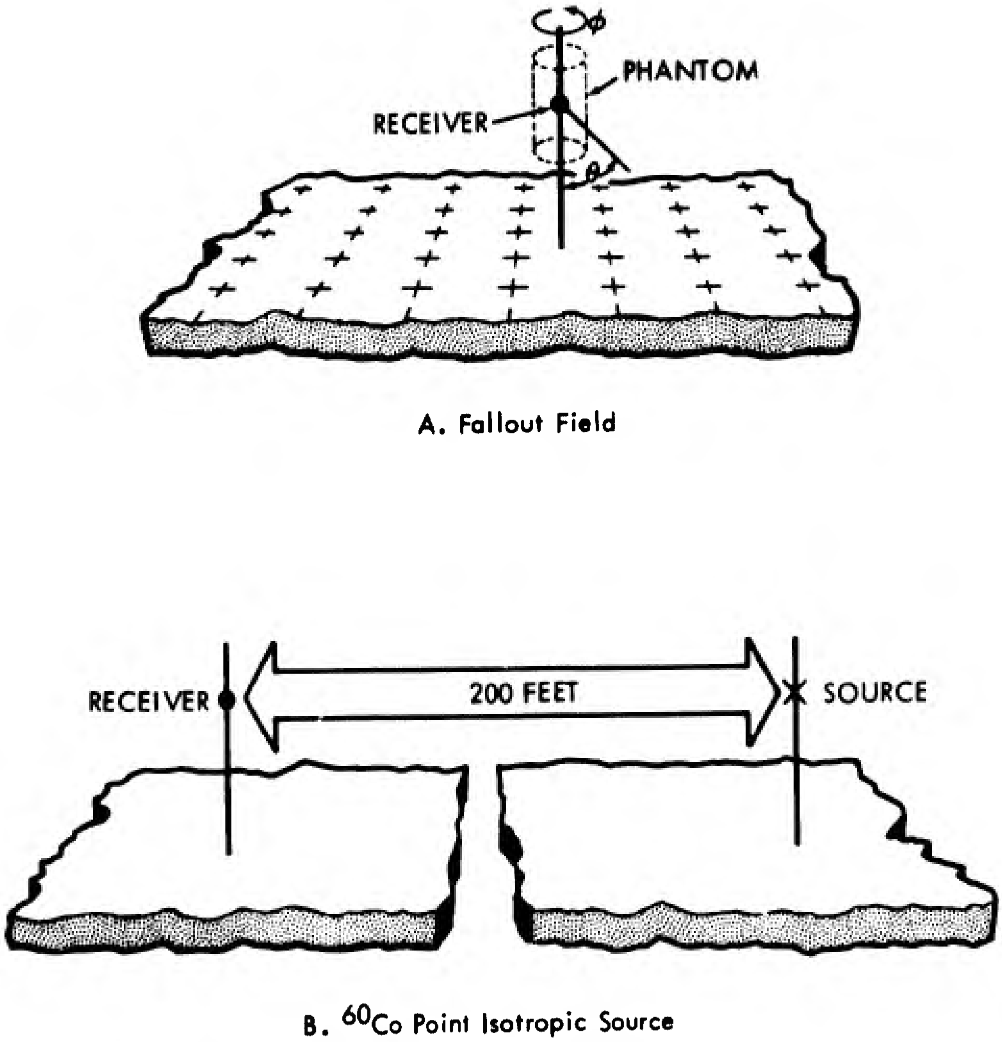

Figure 1. Geometry Assumed for Fallout and ^{60}Co Point Source Radiation Environment Calculations

area on the infinite plane source. These point sources were carefully positioned to obtain a smooth integration and extended to a distance of 1600 ft from the receiver.

In a point isotropic source calculation, the L05 Monte Carlo Program selects source emission directions at random and follows each photon through a path or random walk generated by random sampling from collision probability distributions and scattering angle distributions for the material being penetrated. Upon each collision, statistical estimation is applied to compute the probability that the scattered photon will go directly from the scattering center to the receiver without further interaction. These probabilities are scored at the receiver according to the photon's energy and the angle through which it arrives. An adequate number of photon paths or "histories" must be computed to insure a representative distribution of scattering events in the media about the source and receiver. The Monte Carlo estimate of the flux density at the receiver is then the sum of the probabilities accumulated from all histories divided by the total number of histories.

For the fallout calculation, a total of 23,000 histories were run (2,300 for each source energy). These numbers were generally adequate to keep the indicated standard deviation of the total flux density for each source energy below 10 percent. Each photon history was terminated upon the 15th collision or upon the photon energy being degraded below 0.04 MeV.

The results of the fallout calculations were found to compare favorably with those of other investigators, both experimental[1,2] and theoretical.[14] The results from the fallout radiation environment calculations that were used as input to the depth-dose calculations are given in Tables A1, A2, A3 and A4 of the appendix for fallout ages of 1.12 hrs, 23.8 hrs, 4.57 days and 9.82 days, respectively. In these tables, the photon flux densities are listed for each energy-angle bin. Also tabulated is the total flux density in each energy bin (summed over all angles) and in each angle bin (summed over all energies), tissue dose rate as a function of angle, and the total flux density and tissue dose rate at the receiver point.

2.2 Simulated Fallout

The radiation environments of fallout as simulated by the ^{60}Co point isotropic source for several source-receiver separation distances and by the AFRRI Compact Simulator were calculated by the L05 Monte Carlo procedure.[18]

The geometry for the ^{60}Co point isotropic source is shown in Figure 1B. Of those distances examined, the separation distance of 200 ft for the source was selected because it best approximated the energy and angle distribution from an infinite plane fallout source. The flux densities at the receiver were sorted into the energy and angle groups described above for the fallout calculations. As was the case for fallout, the flux densities were integrated over the azimuthal angle, ϕ. Thus the environment computed for the ^{60}Co point source is that which would be experienced by a subject rotated on its vertical axis during exposure. The scattered components of the computed flux densities which were used as input to the depth-dose calculations are given in Table A5 of the appendix. The uncollided component, 1.362×10^{-9} photons/cm^2-sec per source photon/sec, was taken from Table I of Reference 18.

The AFRRI Compact Simulator, which is a conceptual design, consists of a uniform disc source located on the ground surface, a ring source above the perimeter of the disc source, and a slab of water of equal radius positioned above and concentric with the disc and ring sources. The geometry is shown in Figure 2. The ring source serves as a virtual source for that portion of an infinite plane source not included within the finite disc source while the water serves as a scattering medium for gamma rays from

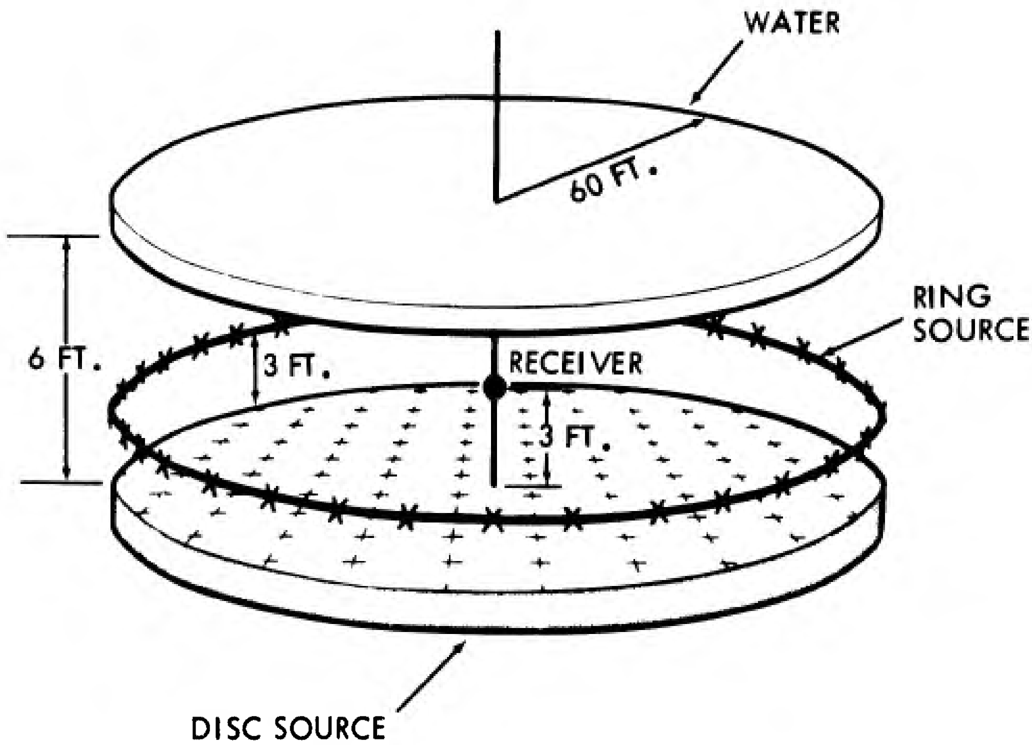

Figure 2. AFRRI Compact Simulator

both the disc and ring source to simulate skyshine from an infinite plane source. The relative concentrations of the ^{60}Co, ^{137}Cs and ^{144}Ce in the disc and ring sources and the thickness of the water slab were selected to give the best approximation of the energy and angle distributions 3 ft above 1.12-hr fallout.

The radiation environment of the AFRRI Compact Simulator used for the depth-dose calculations was that computed for a receiver located on the axis and 3 ft above the disc source (Table A6 of the appendix). It was found in the original study, however, that the simulator produced substantially the same environment at positions located off of the axis by as much as 30 ft.

The characteristics of the 1.12-hr fallout and the simulated fallout radiation environments are compared in Figure 3. The angle distributions of the total dose rate in tissue given in Figure 3A, have the same gross shape for $\theta > 80$ degrees; but below 80 degrees, the ^{60}Co angle distribution bears no resemblance to that from fallout. Neither the AFRRI Compact Simulator nor the ^{60}Co point source provides a good simulation of the free-field energy spectra of fallout as may be seen in Figure 3B. This deficiency results from the complete lack of photons with energies greater than 1.33 MeV from the simulator sources, although such photons are relatively abundant in actual fallout.

2.3 Foxhole

The geometry of the 4 ft diameter by 5 ft deep foxhole is shown in Figure 4. The radiation field in the foxhole may be classified into three components. The "air-scattered" component is that which has scattered in air above the ground and enters the foxhole, reaching the receiver without further collision. The "wall-scattered" component contains all photons which have scattered from the foxhole wall or floor before reaching the receiver. Lastly, the "uncollided" component is that which emanates from the fallout source on the ground and penetrates the foxhole lip to

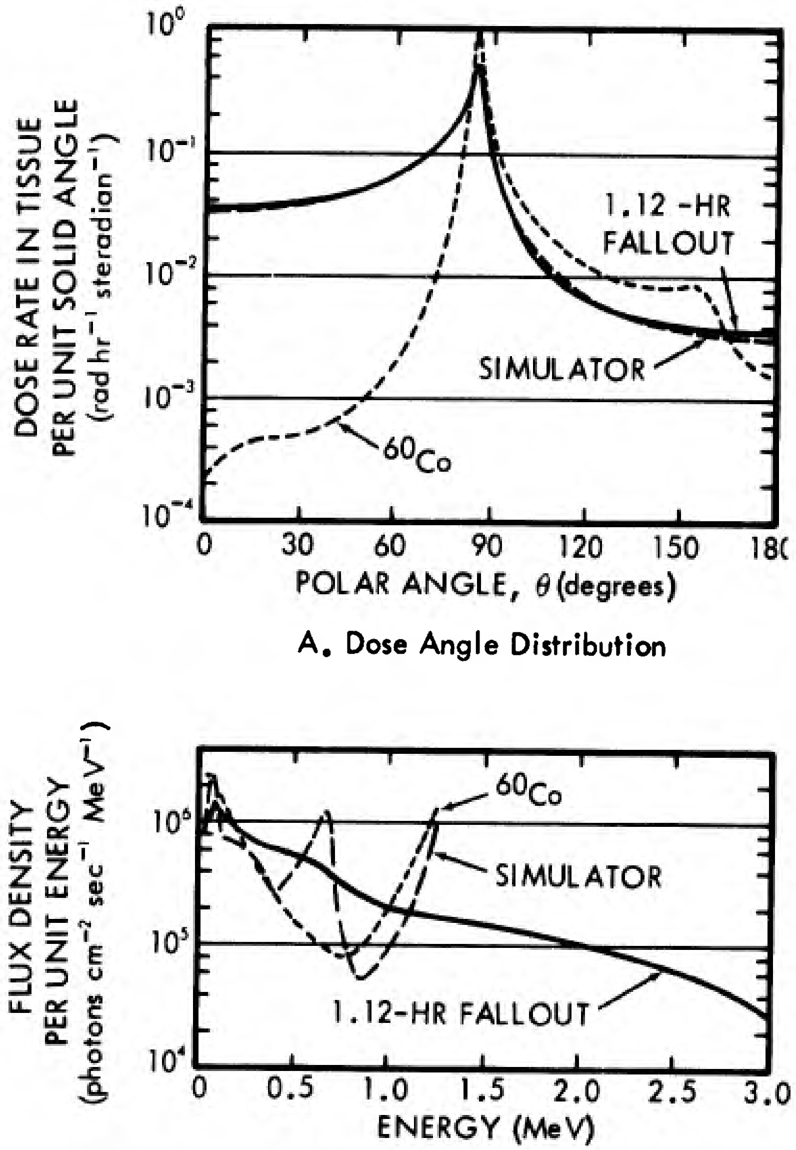

A. Dose Angle Distribution

B. Energy Distribution

Figure 3. Gamma-Ray Energy and Angle Distributions from 1.12-Hr Fallout, ^{60}Co Point Source, and AFRRI Compact Simulator (normalized to unit dose rate)

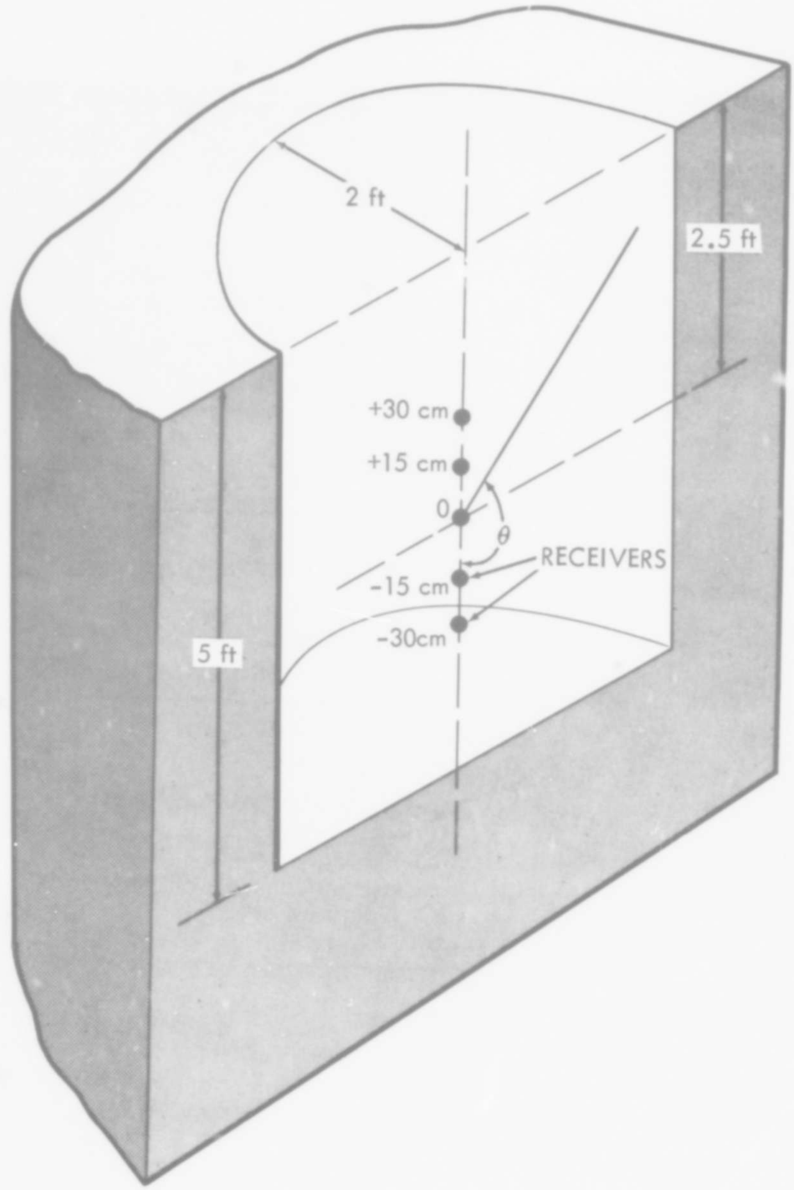

Figure 4. Foxhole Geometry

arrive at the receiver without suffering a collision. All three components were considered in generating the photon energy and angle distributions on the surfaces of the phantom.

The uncollided component was computed by straight-forward analytical means. The air-scattered component was derived from the above-ground free-field case by assuming the foxhole was, in effect, a collimator. The wall-scattered component consists of air-scattered photons which enter the foxhole through its aperture and subsequently scatter from the wall or floor and those which first undergo a collision in the ground and then enter the foxhole through the wall or floor. The latter constitute a small fraction of the total wall-scattered component (which itself contributes less than 10 percent to the total flux density in the foxhole) and was ignored. The former was computed with the L05 Monte Carlo procedure[21] assuming the energy and angle distribution of the "collimated" above-ground free-field results as a source term for the photons incident upon the walls and floor.

The original foxhole calculations[18] were performed for only one receiver - that located on the axis 2.5 ft below the ground plane. Since the radiation environment may be expected to vary considerably with position in the foxhole, it was necessary in the present study to perform calculations for the additional receiver positions shown in Figure 4. During the course of these calculations, it was discovered that an error had been made in the original wall-scattering calculations for the 2.5-ft position. The error resulted from an error in converting the photon flux density to an equivalent area source in defining the pseudo-source term for the wall-scattering calculations. Corrected calculations were performed which reduced the contribution of the wall-scattered component at the center receiver from 24.8 to 5.1 percent of the total dose rate.

Although calculations were performed explicitly for the air-scattered and uncollided components at the added receiver positions in the foxhole, the corrected wall-scattered component computed for the center position was assumed to apply at the new positions. This assumption was justified by simplifed albedo calculations which indicated that the wall-scattered dose rate at the new receiver positions should not vary by more than approximately 25 percent from that at the center position. Further justification stems from the fact that the wall-scattered component is only 5.1 percent of the total at the center position.

The energy and angle distribution of the photon flux density at each of the five receiver positions in the foxhole are given in Tables A7 through A11 of the appendix. These data were used to define the photon distributions incident upon the phantom in the depth-dose calculations.

III. METHODS

For the depth-dose calculations, the phantom was superimposed over the point receiver locations for which the free-field radiation environments were obtained. In the above ground cases, the axial midpoint of the phantom was placed 8 in. above the point receiver and hence, 3 ft, 8 in. (111.8 cm) above the ground surface. In the foxhole the phantom midpoint was located at the midpoint of the foxhole axis 2 ft 6 in. below the ground surface.

The phantom used in the calculations was a torso model consisting of a tissue equivalent vertical right cylinder of 60 cm height and 30 cm diameter. For tissue equivalence, the phantom was composed of a homogeneous mixture of the elements indicated in Table I.

Table I. Composition of Tissue Equivalent Phantom

Element	Percent by Weight	Partial Density ($gm\ cm^{-3}$)	Atomic Concentration ($atoms\ cm^{-3}$)
Carbon	15.6	0.1585	7.944×10^{21}
Hydrogen	9.8	0.0996	5.948×10^{22}
Oxygen	71.0	0.7214	2.714×10^{22}
Nitrogen	3.6	0.0366	1.573×10^{21}
Total	100.0	1.0161	9.614×10^{22}

To compute the distribution of the gamma-ray dose in the phantom, it is necessary to consider the gamma rays incident over its entire surface and their transport until they are absorbed in, or escape from, the phantom. In the above-ground cases photons which escape the phantom may be scattered back into it, but because of the small size of the phantom compared to the scattering mean-free-path in air, the probability of this occurring is so small that it may be safely neglected. In the foxhole, this assumption is not as easily justified because of the proximity of the foxhole walls. Although these "re-entering" photons would occur with greater frequency, solid angle and albedo considerations indicate that they would comprise no more than 2 percent of the total incident flux density. Therefore, they were also neglected.

In performing the radiation transport calculations, the photon flux density as a function of energy must be determined at a suitable number of positions in the phantom to allow, after conversion to dose, construction of dose or dose fraction profiles. The Monte Carlo procedure used to perform the depth dose calculations is a multi-purpose code package known as COHORT.[22,23] Section 3.1 gives a brief description of COHORT with emphasis on those features actually used in the present study. The reader is referred to the COHORT documentation for a more complete description.

The input data and parameters used in the Monte Carlo calculations and the procedures used in the reduction of the Monte Carlo results to the desired form are described in Section 3.2. The simplified analytic methods used for the exploratory depth-dose calculations in the above-ground geometries are described in Section 3.3.

3.1 COHORT Description

The principal codes of the COHORT package are the SOURCE (S01 and S02), HISTORY (H01), and ANALYSIS (A01 and A02) codes. Figure 5 illustrates the functions and relationships of the principal codes.

The S01 code is used to generate the initial parameters defining the spatial distribution, direction, energy and weight of primary gamma rays or neutrons. The S02 code, not used in the depth-dose study, generates a similar set of parameters for secondary gamma rays using as input neutron distribution data from a previous COHORT calculation.

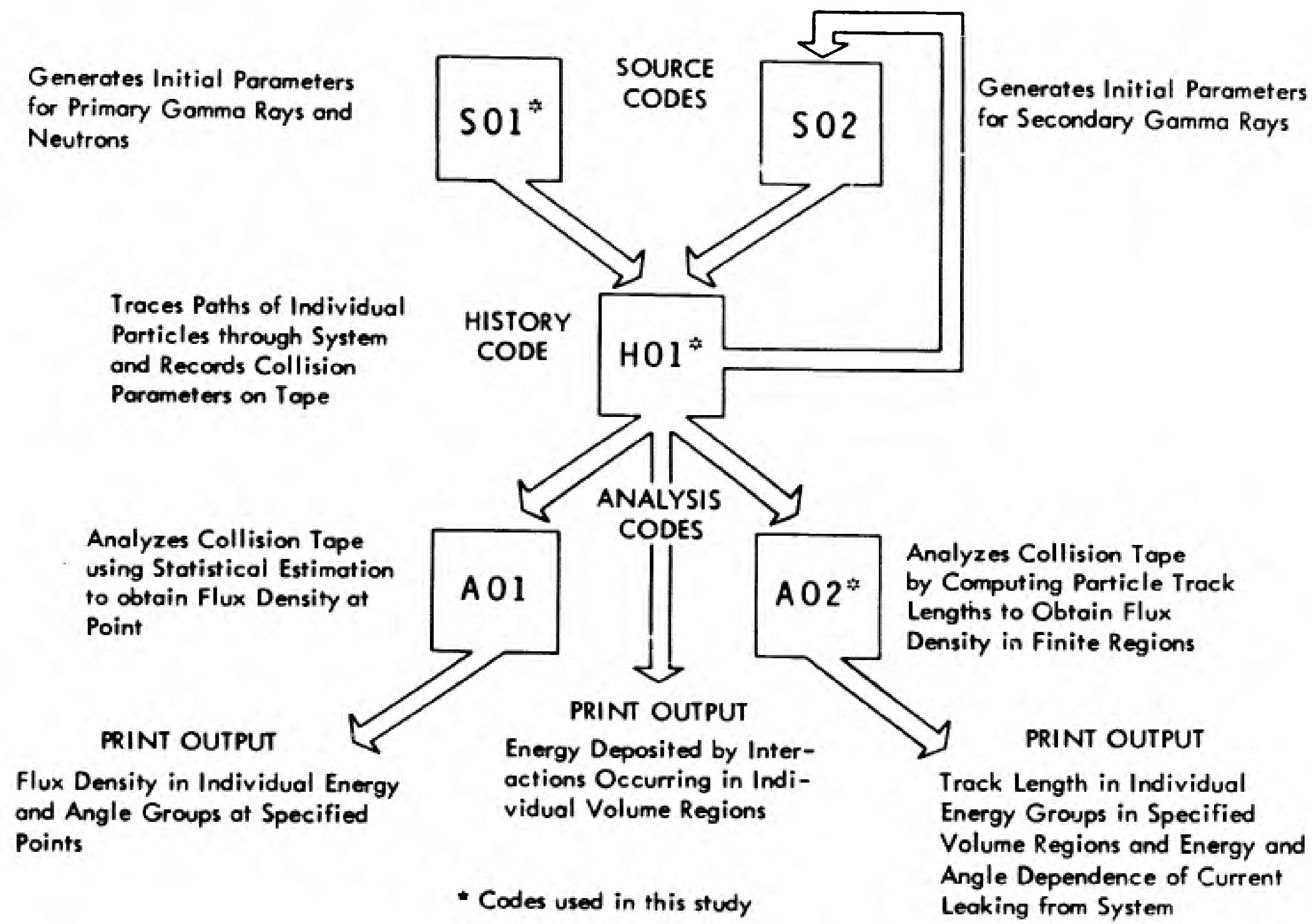

Figure 5. Function and Relationship of the Principal Codes of the COHORT Package

The basic assumption in the S01 code is that the distribution defining the source can be separated into independent distributions which define the spatial, direction, and energy parameters. To obtain specific starting parameter values for each particle whose history is to be traced, Monte Carlo techniques are used to draw samples from the specified probability distributions. For the depth-dose calculations, photons must be started inward from a pseudo-source covering the phantom when it is exposed to the desired radiation field. Although S01 could handle the depth-dose calculations, each calculation would have to be broken into a number of individual problems because of the above-mentioned restriction requiring independent spatial, direction and energy distributions.

Thus, to reduce the amount of external data handling in the depth-dose calculations, S01 was modified to accept as direct input the free-field gamma-ray energy and angle distributions assumed to be incident upon the phantom, and to compute the necessary probability distributions from these data. The code was also revised to perform correlated rather than independent sampling from these distributions. This special version of S01, designated RRA-62,[24] differs from the regular version only in the input data formats and in the routines used for cylindrical volume sources with an anisotropic angle distribution.

The operation of the Modified S01 code in generating photon starting parameters corresponding to exposure to a given radiation field may be summarized as follows:

1. From the input energy and angle distribution and the phantom dimensions, the fractions of the total number of photons which enter the bottom, side (lateral) and top phantom surfaces are computed. These fractions are used as probabilities in determining which surface a given photon enters.

2. If the photon is started from the top or bottom surface, its spatial coordinates are selected assuming a uniform probability distribution over the surface.
3. If the photon is started from the lateral surface, its spatial coordinates are selected from a uniform distribution on azimuth and from a height distribution specified in the input.
4. The energy distribution of the photon current entering each of the three surfaces of the phantom is computed in the form of a probability distribution which is sampled to assign an energy to the photon entering the surface.
5. The polar angle (θ) distribution of the photon current within each energy group for each surface is computed. The distribution, expressed as a set of probabilities for the appropriate surface and energy group, is sampled to obtain a particular polar angle for the photon.
6. If the photon is started from the top or bottom surface of the phantom, its azimuthal angle (ϕ) is assigned by sampling from a uniform distribution; if from the lateral surface, the sampling is from a cosine distribution.
7. The procedure assigns weights to individual photons such that the results will be normalized to unit free-field dose rate.

The S01 code records the starting parameters for the required number of photon histories on a "source tape" that is used as input to the H01 code. Additional input required for H01 is the geometry of the phantom and energy-dependent cross-section data for each element included in the phantom.

The H01 code traces the paths of individual photons through a random walk generated by sampling from collision probability distributions and scattering angle distributions for the phantom materials. The collision probability distributions are generated from consideration of the cross sections for Compton scattering, pair production and absorption. Absorption is not allowed to terminate a walk. Instead, the photon weight is reduced upon each interaction by the probability that the particular interaction was an absorption. The scattering angle distributions are generated from the well-known Klein-Nishina formula. Each photon history is terminated upon reaching a specified minimum energy, a specified maximum number of collisions, or escaping from the defined geometry.

In the process of tracing photon histories, the location of each interaction and the resultant photon energy and direction are recorded on tape. The resultant "collision tape" from H01 may then be analyzed by the A01 or A02 codes to determine the photon flux density at specified positions. Additional output from H01 includes the amount of energy deposited in arbitrarily defined volume regions of the phantom through photon collision and photon absorption. This output is of limited usefulness in the depth-dose study, however, because an excessive number of photon histories must be traced to obtain a suitable degree of spatial resolution.

The "collision tape" output from H01 may be analyzed in various ways to obtain the desired results from the transport calculations. The A01 analysis code, which uses statistical estimation to determine the scattered flux density in arbitrary energy and angle groups at specified point receiver locations, was not used in the depth-dose study.

The A02 analysis code, which was found to be the best suited to the depth-dose study on the basis of information yielded and cost considerations, computes the "expectation" track length in each volume region which is intercepted by a projection of each photon flight from a collision. These track lengths are sorted according to volume region and photon energy. An estimate of the average photon flux density in a given region may then be obtained by dividing the total track length in that region by the region volume.

One of the advantages of A02 over A01 is that it includes the flux density contribution from uncollided photons since the initial flight of a photon from its point of origin is included. The A02 code was modified for this study to compute the dose deposited in each volume region by multiplying the flux density contributed by each photon track by a flux-to-dose rate conversion factor[25] supplied as input and then summing over-all energy groups.

3.2 Monte Carlo Depth-Dose Calculations

The S01 calculations were relatively straightforward for the above-ground cases. For these cases, the free-field energy and angle distribution tables given in the appendix were used as input for the special version of S01. Special calculations of the total flux density above a 1.25-MeV plane isotropic source showed that it varied by 12 percent over the height of the phantom. In the depth-dose calculations it was assumed that the incident flux density from all of the sources except the ^{60}Co point source had a similar height dependence. No such adjustment is required for the ^{60}Co source geometry. To make a first order correction for this dependence, the phantom's lateral surface was divided into five equal intervals and the appropriate probability was input for each. The relative energy and angle distribution of the free-field flux density was assumed not to vary over the height of the phantom.

A special treatment was required for the foxhole case since the height dependence of the energy and angle distribution could not be neglected. This treatment consisted of dividing the phantom's lateral surface into five intervals and using a different angle distribution for each. Each lateral interval was further divided into six subintervals and different probabilities were input for each to account for the vertical dependence of the total flux density. It should be noted that the five source distributions for the phantom's lateral surface, generated along the axis of the foxhole at the receiver locations shown in Figure 4, were assumed to be valid on the lateral surface, 6 in.off the axis. As discussed below, the depth-dose distributions are not sensitive to differences in the energy and angle distributions; thus the approximation appears to be reasonable.

The H01 and A02 calculations were performed in a straightforward manner, and no special treatment was required for the foxhole. The only thing which differed from run to run were the data on the source tapes for H01 and on the collision tapes for A02. The cross sections used for these calculations were taken from Grodstein's compilation.[20] The library used contained values for 85 energies in the interval 0.01 to 3.64 MeV.

The volume regions into which the phantom was divided for the H01 and A02 calculations are shown in Figure 6 and listed in Table II. Also given in Table II are the region volumes and the location of the midpoint of each region. The volume regions are concentrated along the horizontal midplane and the vertical axis since it was desired to compute the radial and axial distributions of the dose. The dimensions of the volume elements are smallest near the phantom surface where the largest dose gradients were expected.

Ideally, the volume regions would be of small size to obtain a high resolution of the spatial dependence of the dose. In order to obtain valid results, however, each region had to be large enough to intercept a statistically significant number of photons. The regions shown in Figure 6 were arrived at through exploratory calculations and represent a compromise among several considerations including spatial resolution, statistical accuracy, and computing economy.

The principal factor affecting the statistical accuracy of the Monte Carlo calculations was, of course, the number of photon histories traced in the H01 runs. Exploratory calculations led to the selection of 10,000 photon histories as the minimum problem size to give acceptable statistical accuracy. To further improve the statistical accuracy, four different computer runs of approximately 10,000 histories each, using different random number

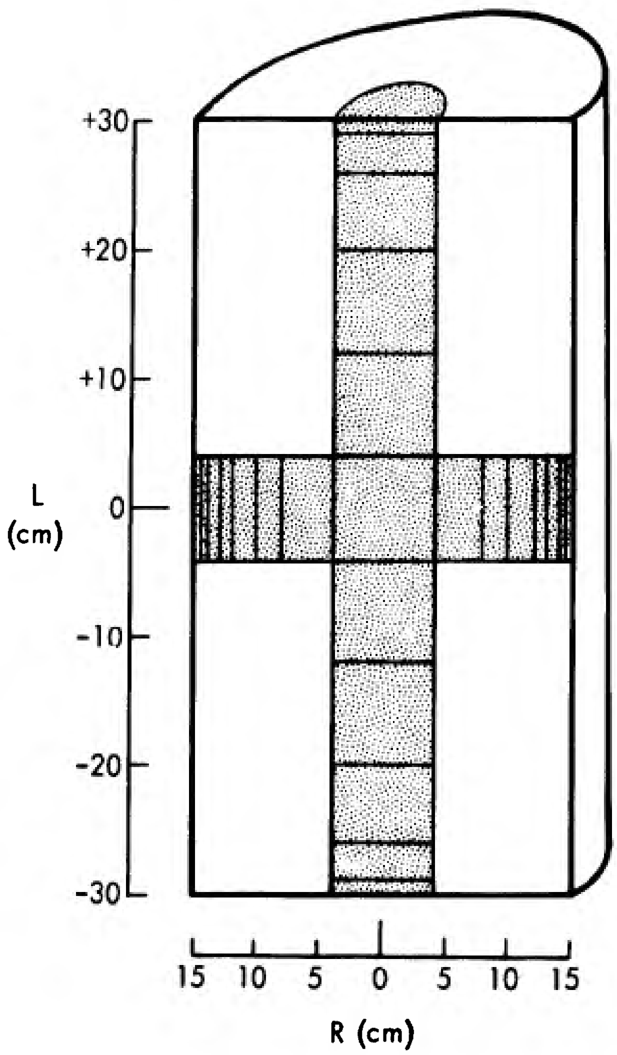

Figure 6. Division of Phantom into Volume Regions for Monte Carlo Calculations

Table II. Volume Regions of Phantom

Axial (L) Distribution				Radial (R) Distribution			
Lower Boundary L_1(cm)	Upper Boundary L_2(cm)	Volume (cm^3)	Midpoint $\overline{L}$ (cm)	Inner Boundary R_1(cm)	Outer Boundary R_2(cm)	Volume (cm^3)	Midpoint* $\overline{R}$ (cm)
-30	-29	50.3	-29.5	0	4.0	402.1	2.83
-29	-26	150.8	-27.5	4.0	8.0	1206.4	6.32
-26	-20	301.6	-23.0	8.0	10.0	904.8	9.06
-20	-12	402.1	-16.0	10.0	12.0	1105.8	11.04
-12	- 4	402.1	- 8.0	12.0	13.0	628.3	12.51
- 4	+ 4	402.1	0	13.0	14.0	679.0	13.51
[Volume Regions for L>+4 are mirror				14.0	14.5	358.1	14.26
images of those for L<-4.]				14.5	15.0	370.7	14.75

* $\overline{R} = \left[\frac{1}{2}\left(R_2^2 + R_1^2\right)\right]^{1/2}$

sequences, were made for each problem. The final results for most positions in the phantom had standard deviations of less than 5 percent.

In performing the Monte Carlo calculations, each photon was allowed to undergo 25 collisions or be degraded in energy to less than 0.04 MeV before termination. However, it was found that approximately 96 percent of all photon histories were terminated by escape from the phantom. Only 3 percent and 1 percent were terminated by minimum energy and maximum number of collisions, respectively. An average of only 3.8 collisions were suffered by each photon before its history was terminated.

The print output taken from the A02 runs consisted of the total photon track length in each volume region and in each of ten energy groups:

0.04 - 0.06 MeV
0.06 - 0.10
0.10 - 0.18
0.18 - 0.30
0.30 - 0.50
0.50 - 0.75
0.75 - 1.00
1.00 - 1.50
1.50 - 2.50
2.50 - 3.50

The photon flux density in each energy group was obtained by dividing the track length by the volume of the region. The dose rate in each region was obtained by multiplying the photon flux density in each energy group by the corresponding flux-to-dose rate (in tissue) conversion factor[25] and then summing over energy. The dose rate thus computed for each region may be regarded as a "dose fraction"* since the source strength normalization is to the unit free-field dose rate in tissue at the point receiver location.

---

* "Dose fraction" is defined on page 31.

A statistical analysis was performed of the depth-dose distributions from the four different runs made for each case. Standard deviations were computed for each position in the phantom using the equation

$$S = \sqrt{\frac{\sum_{n=1}^{n=K} (\delta X_n)^2}{K-1}}$$

where δX_n is the difference between the dose fraction for the n^{th} run and the average of all runs.

3.3 Analytic Calculations*

Previous studies indicate that approximately 80 to 85 percent of the free-field dose at a position 3 ft above an infinite plane fallout source is from uncollided photons. Hence, most of the dose near the phantom surface results from the first collision of the uncollided photons incident upon the phantom. Moreover, exploratory calculations for a representative photon energy of 1.25 MeV indicated that approximately one-half of the dose rate at the center of the phantom is from photons which have suffered no prior collision in either air or ground or in the phantom. Because these uncollided photons contribute a large fraction of the total dose, a FORTRAN procedure was developed to perform separate analytic calculations for this component. Infinite water dose build-up factors were incorporated in the procedure to provide an approximation of the dose from higher collisions in the phantom, and provision was also made for allowing the fallout to be buried at an arbitrary depth below the ground surface to give an approximation of the ground roughness effect.[26] This FORTRAN procedure, designated RRA-57, was designed to treat individual source energies separately so that the results could be weighted and combined for arbitrary fallout energy spectra.

---

* These analytic calculations were performed for the above-ground case only.

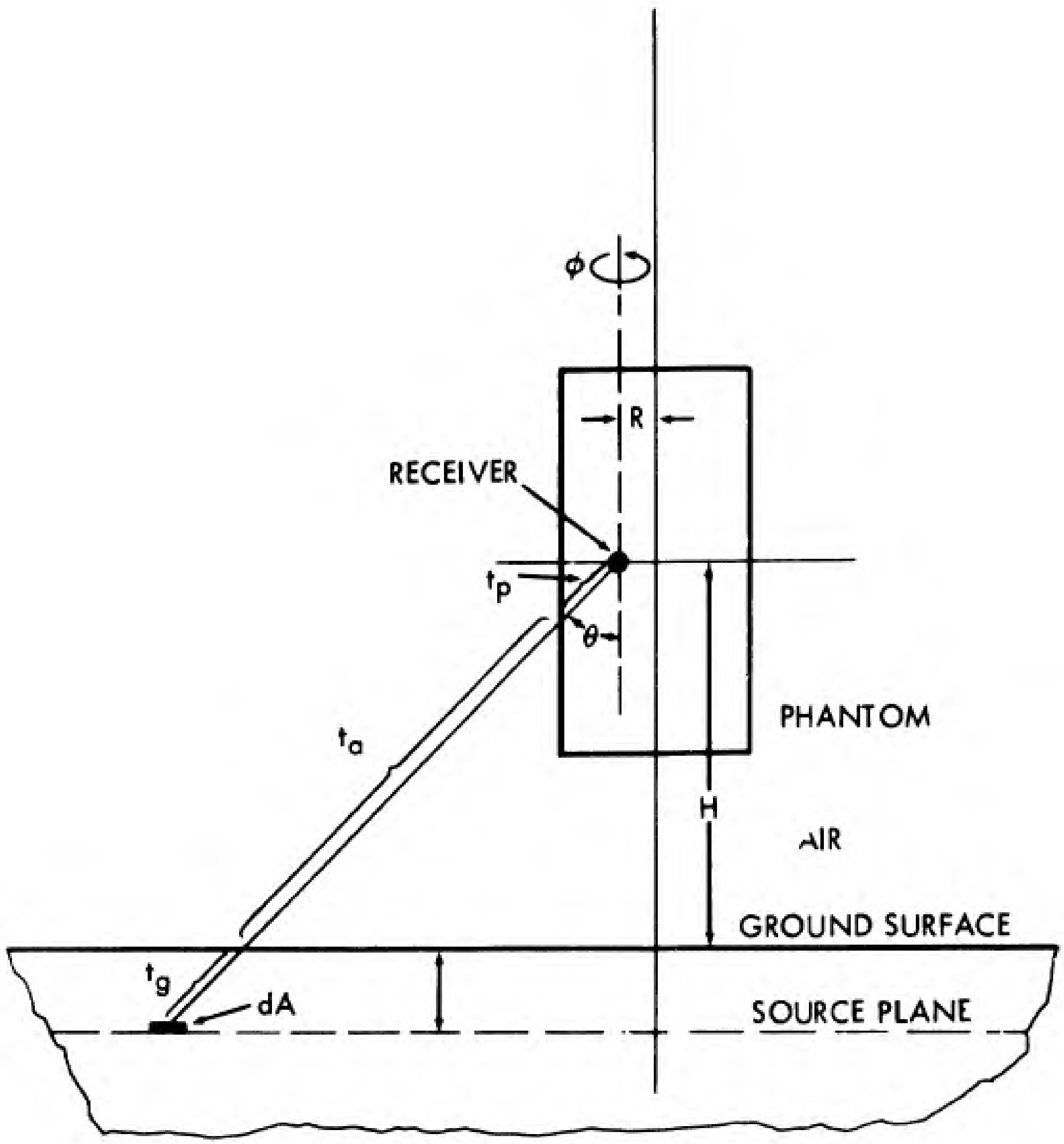

Figure 7. Geometry for Calculating Uncollided Flux Density in Phantom from a Fallout Source

The geometry is shown in Figure 7. The uncollided flux density at a receiver position in the phantom from a differential area, dA, on the plane isotropic monoenergetic source emitting one photon per unit time per unit area is

$$dF = \frac{e^{-(\mu_g t_g + \mu_a t_a + \mu_p t_p)}}{4\pi(t_g + t_a + t_p)^2}\, dA$$

where μ_g, μ_a and μ_p are the linear attenuation coefficients of the ground, air and phantom, respectively, and t_g, t_a and t_p are the path lengths in the ground, air and phantom, respectively.

Expression of dA in terms of θ and ϕ leads to the following equation for the dose rate of the uncollided component at the receiver:

$$D_D = \frac{G}{2\pi} \int_0^{\pi} \int_0^{\pi/2} e^{-(\mu_g t_g + \mu_a t_a + \mu_p t_p)} \tan\theta\, d\theta\, d\phi$$

where G is the flux-to-dose rate (in tissue) conversion factor.[25]

An approximation of the dose rate at the receiver from photons scattered in the phantom but not in air or ground is

$$D_S = \frac{G}{2\pi} \int_0^{\pi} \int_0^{\pi/2} [B(\mu_p t_p) - 1] e^{-(\mu_g t_g + \mu_a t_a + \mu_p t_p)} \tan\theta\, d\theta\, d\phi$$

where $B(\mu_p t_p)$ is the dose buildup factor for a point isotropic source in an infinite water medium.[27]

In order to obtain an idea of the accuracy of the RRA-57 scattered dose calculation, the ratio of the total dose (from uncollided plus phantom-scattered photons) to the dose from uncollided photons was computed for several radial positions in the phantom midplane and compared with similar ratios computed with the L05 Monte Carlo procedure.[21] These ratios may be called "phantom buildup factors". The L05 calculations considered the finite geometry of the phantom and assumed a monoenergetic, isotropic source uniformly distributed over the lateral surface of the phantom, whereas the RRA-57 calculations assumed the source to be uniformly distributed over the ground surface and used infinite water buildup factors.

The L05 and RRA-57 phantom buildup factors for several source energies are compared in Table III. In most cases they agree within 10 percent and the difference is less than 25 percent in the worst case. It was expected that the agreement would be worse near the lateral surfaces of the phantom since the infinite medium buildup factors do not account for boundary effects as do the L05 calculations. In regions close to the phantom's lateral surface, the analytic approximation underestimates the scattered contribution from photons entering the phantom near the region since $B(\mu_p t_p)$ approaches 1 as $\mu_p t_p$ approaches 0. However, this effect appears to be offset by the fact that the contribution in the region from photons penetrating a significant portion of the phantom is overestimated by infinite medium buildup factors. It should also be noted that the effect of the difference in the source distributions between the RRA-57 and L05 calculations is not known and may also tend to offset or obscure the boundary effects.

Table III. Comparison of Phantom Dose Buildup Factors Computed with RRA-57 and L05

Receiver Location, R (cm)	Source Energy (MeV)							
	0.25		0.67		1.25		2.50	
	A-57	L05	A-57	L05	A-57	L05	A-57	L05
0	7.04	7.40	3.11	2.55	2.04	1.95	1.51	1.46
4	6.55	5.80	2.95	2.51	2.00	1.88	1.49	1.46
8	4.93	4.41	2.55	2.30	1.84	1.74	1.42	1.42
11	3.58	3.46	2.15	1.96	1.66	1.56	1.35	1.34
14	2.18	2.22	1.61	1.43	1.39	1.25	1.23	1.17

A second FORTRAN procedure, designated RRA-58, was prepared to calculate the dose in the phantom resulting from radiation which has scattered before striking the phantom. This procedure is similar to the one described above, the principal difference being that the "source" is an arbitrary photon energy and angle distribution incident upon the phantom. Consider photons incident upon the phantom with a given energy in a polar angle interval $\theta_1 - \theta_2$ (see Figure 7). Assuming azimuthal symmetry and a uniform distribution of photons within the polar angle interval, the equation for the fraction A of the incident photons which penetrate without interaction to the receiver is

$$A(\theta_1 - \theta_2) = \frac{1}{\pi(\cos\theta_1 - \cos\theta_2)} \int_0^{\pi} \int_{\theta_1}^{\theta_2} e^{-\mu_p t_p} \sin\theta d\theta d\phi$$

where: μ_p = linear attenuation coefficient of phantom

t_p = total path in the phantom to a given receiver position for a ray incident with angles θ and ϕ.

The gamma-ray dose buildup factor is given by

$$B(\theta_1 - \theta_2) = \frac{\frac{1}{\pi(\cos\theta_1 - \cos\theta_2)} \int_0^{\pi} \int_{\theta_1}^{\theta_2} B(\mu_p t_p)\, e^{-\mu_p t_p}}{A(\theta_1 - \theta_2)} \sin\theta d\theta d\phi$$

Using the above equations, the RRA-58 procedure computes a set of attenuation factors $A_{\bar{\theta},E}$ and buildup factors $B_{\bar{\theta},E}$ for each angle interval $(\theta_1 - \theta_2)$ about $\bar{\theta}$ and each energy group E. The attenuation factors, along with the flux-to-dose rate conversion factors, are folded with the free-field scattered photon energy and angle distributions to obtain the uncollided component in the phantom due to incident air- and ground-scattered photons. Similarly, the buildup factors are folded in, and the portion scattered in the phantom is obtained by subtracting the uncollided component from the total.

IV. RESULTS AND COMPARISONS

The principal results of the Monte Carlo and analytic calculations are summarized in Tables IV and V respectively. Doses in the phantom are expressed as "dose fractions"; the fraction of the free-field dose rate in tissue at the point receiver positions over which the phantom was superimposed.

The results of the various calculations were analyzed to determine:

1. The general characteristics of the depth-dose distributions in the phantom.
2. The sensitivity of the distributions to fallout age.
3. The extent to which the simulated fallout fields reproduce the fallout depth-dose distributions.
4. The validity of the simplified analytic calculations.

The analysis was accomplished through comparison of the results given in Tables IV and V and through examination of auxiliary results given elsewhere in this chapter.

4.1 Comparison of Depth-Dose Distributions

The case of principal interest is the 1.12-hr fallout field since this particular age of fallout has been studied extensively.[14,17,18] Figure 8 compares the Monte Carlo and analytic calculations for this case. The Monte Carlo standard deviations on the radial distribution are quite small (~2 to 8 percent). Owing to the use of much smaller volume regions, the standard deviations on the axial distribution are larger near the bottom and the top of the phantom.

The Monte Carlo results indicate a dish-shaped radial distribution with a dose fraction of 0.81 near (0.5 cm) the lateral surface of the phantom as compared to one of 0.66 at the center. For $-20<L<+20$ cm, the axial distribution is approximately a straight line which closely follows the height-above-ground dependence of the free-field dose rate.

Table IV. Depth-Dose Distributions Based on Monte Carlo Calculations

(dose fraction)

Position L or R (cm)	Source: 1.12-hr Fallout		23.8-hr Fallout		AFRRI Compact Simulator		^{60}Co Point Source		Foxhole*	
Radial Distribution										
2.83	0.6571±	8.14%**	0.6848±	3.59%	0.6418±	7.14%	0.6684±	5.05%	0.6096±	4.24%
6.67	0.6701	2.19	0.6673	2.91	0.6600	2.44	0.6828	3.86	0.5944	3.24
9.06	0.6955	1.55	0.6782	0.18	0.6806	2.23	0.6997	3.86	0.5932	1.40
11.04	0.7126	2.87	0.7173	2.20	0.7190	0.71	0.7236	3.95	0.6268	8.39
12.51	0.7621	5.35	0.7173	2.76	0.7676	1.30	0.7540	3.66	0.6564	6.34
13.51	0.7687	4.31	0.7405	2.44	0.7547	3.93	0.7584	1.57	0.6922	4.50
14.26	0.7067	3.49	0.7500	3.16	0.7724	4.40	0.7717	2.63	0.7253	1.60
14.75	0.8114	2.33	0.7844	6.03	0.7812	3.04	0.7740	5.07	0.7492	1.28
Axial Distribution										
-29.5	0.9357±	25.50%	0.9023±	9.65%	0.9132±	18.40%	0.5350±	7.23%	0.2749±	19.75%
-27.5	0.6744	10.54	0.6436	5.16	0.6937	9.34	0.5976	10.27	0.2861	19.50
-23.0	0.7210	4.41	0.6836	8.72	0.6832	5.44	0.6333	7.74	0.3104	9.73
-16.0	0.6860	2.80	0.6443	1.58	0.6393	6.01	0.6500	3.80	0.4154	9.64
- 8.0	0.6926	5.93	0.6452	5.76	0.6380	9.83	0.6809	4.34	0.4268	3.99
0	0.6571	8.14	0.6848	3.59	0.6418	7.14	0.6684	5.05	0.6096	4.24
8.0	0.6382	5.67	0.6500	3.81	0.5818	2.75	0.6611	6.37	0.6698	9.85
16.0	0.6360	4.09	0.6042	9.00	0.5859	4.78	0.6437	6.12	0.9725	7.45
23.0	0.5673	9.94	0.5754	7.05	0.5615	4.86	0.6549	11.68	1.3357	13.68
27.5	0.5305	4.52	0.5253	8.30	0.4873	12.43	0.5782	5.82	1.8356	6.89
29.5	0.5848	15.53	0.4809	14.78	0.4618	18.35	0.6591	12.92	2.0433	19.36

* Phantom located in foxhole exposed to 1.12-hr fallout

** Standard deviation

Table V. Depth-Dose Distributions Based on Analytic Calculations

(dose fraction)

Position L or R (cm)	Source 1.12-hr Fallout	23.8-hr Fallout	4.57-da Fallout	9.82-da Fallout	AFRRI Compact Simulator	^{60}Co Point Source
			Radial Distribution			
0	0.711	0.708	0.717	0.709	0.703	0.740
4	0.718	0.714	0.726	0.716	0.710	0.750
8	0.745	0.743	0.756	0.744	0.732	0.768
11	0.758	0.773	0.786	0.773	0.757	0.789
13	0.793	0.794	0.807	0.803	0.785	0.808
14	0.804	0.801	0.813	0.802	0.788	0.818
15	0.810	0.798	0.808	0.800	0.792	0.826
			Axial Distribution			
-30	0.994	0.983	0.976	0.978	0.994	0.773
-29	0.891	0.906	0.911	0.897	0.898	0.757
-28	0.857	0.872	0.879	0.865	0.864	0.750
-26	0.821	0.832	0.839	0.826	0.825	0.743
-22	0.781	0.786	0.795	0.784	0.781	0.740
-18	0.757	0.761	0.769	0.760	0.756	0.740
-10	0.733	0.733	0.741	0.732	0.726	0.740
0	0.711	0.708	0.717	0.709	0.703	0.740
10	0.693	0.690	0.699	0.691	0.686	0.741
20	0.681	0.679	0.688	0.680	0.574	0.747
30	0.694	0.702	0.715	0.700	0.692	0.802

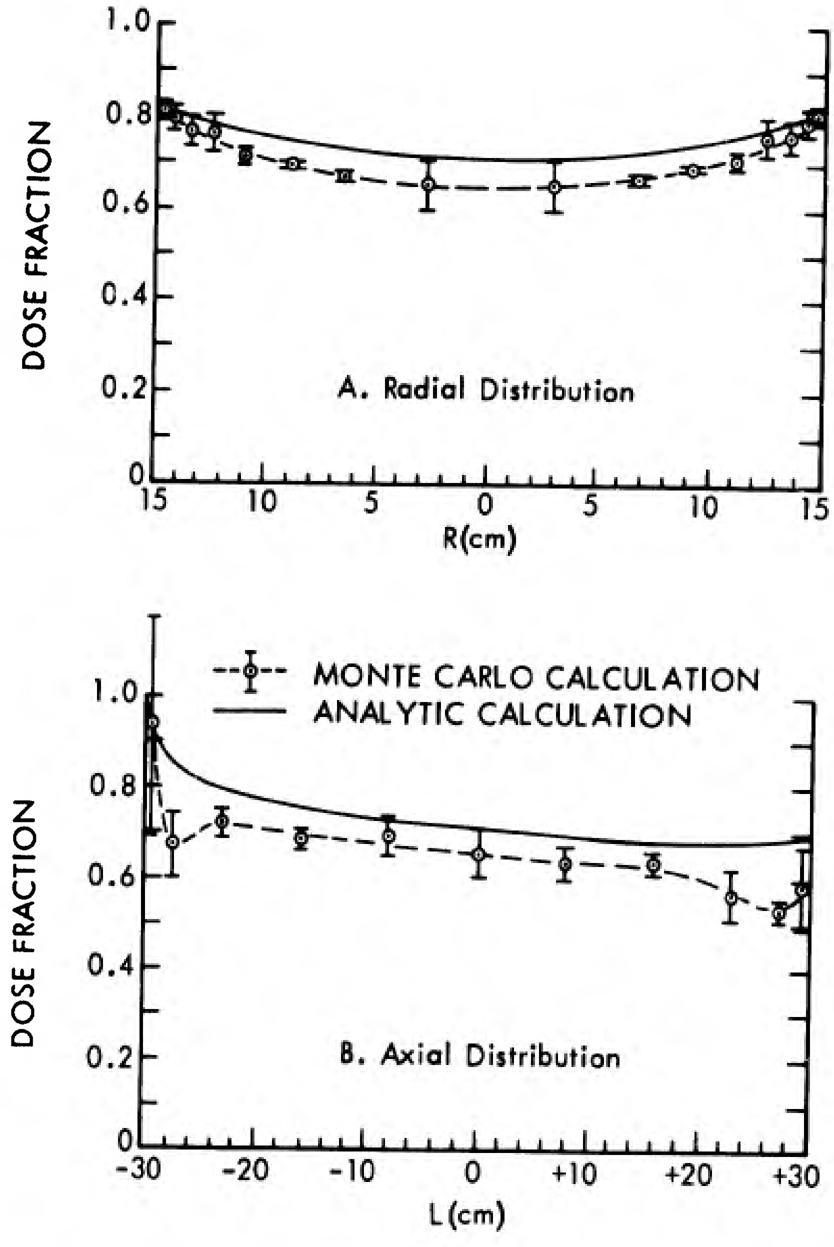

Figure 8. Depth-Dose Distribution in Phantom Exposed to 1.12-Hr Fallout Field

The fine structure in the curve near the upper and lower extremities of the phantom can probably be attributed to the combined effect of the boundaries and of the characteristics of the radiation field. Were it not for the relatively small fraction of low-energy photons which enter through the end surfaces, the dose would be expected to decrease as the end surfaces are approached because of the effect of the boundary on the scattered component. However, the photons entering these end surfaces produce an opposite effect; the fine structure can be attributed to these two effects acting in opposition to one another.

The analytic results differ from the Monte Carlo results in two respects:

1. They tend to give slightly higher (~8 percent) dose fractions in the central regions of the phantom.
2. They do not exhibit the fine structure near the upper and lower extremities.

It was expected that the analytic calculations would generally overpredict the dose fractions owing to the use of infinite medium buildup factors (see Section 3.3). It is perhaps surprising that the overprediction was not larger than 8 percent since the Monte Carlo calculations indicated that the average photon undergoes only 3.8 collisions before escaping from the phantom. However, an analysis (discussed below) of the individual components contributing to the total dose at various positions in the phantom provides some insight into the agreement of the Monte Carlo and analytic calculations.

Table VI lists the percent of the total dose contributed by photons which have 1) suffered no prior collisions in either the air and ground or the phantom (DB-DB), 2) scattered in the phantom but not in the air and ground (DB-PS), 3) scattered in the air and/or ground but not the phantom (AS-DB), and 4) scattered in the air and/or

Table VI. Composition of Gamma-Ray Dose in Phantom Exposed to 1.12-hr Fallout (Analytic Calculations)

(percent of total dose at indicated position)

Position L or R (cm)	Dose Component*			
	DB-DB	DB-PS	AS-DB	AS-PS
	Radial Distribution			
0	43.1	45.3	4.8	6.8
4	44.0	44.0	5.2	6.8
8	47.1	40.8	5.7	6.4
11	51.6	35.9	6.7	5.8
13	56.8	30.2	8.2	4.8
14	61.2	25.5	9.4	3.9
15	67.4	18.9	11.3	2.4
	Axial Distribution			
-30	88.4	0	9.3	2.3
-29	59.3	28.7	7.1	4.9
-28	54.0	34.0	5.9	6.1
-26	49.0	39.2	4.6	6.2
-22	45.6	43.1	4.8	6.5
-18	44.4	44.3	4.7	6.6
-10	43.4	45.2	4.7	6.7
0	43.1	45.3	4.8	6.8
10	43.0	45.0	5.0	7.0
20	42.8	44.7	5.2	7.3
30	41.0	42.8	12.6	3.6

* Dose Components defined as follows:

DB-DB: Incident Direct Beam, Unscattered in Phantom
DB-PS: Incident Direct Beam, Scattered in Phantom
AS-DB: Incident Scattered, Unscattered in Phantom
AS-PS: Incident Scattered, Scattered in Phantom

ground and in the phantom (AS-PS). These data are for 1.12-hr fallout and are based on the analytic calculations. The analytic calculations for the other cases indicated a similar composition. (No such component breakdown is available from the COHORT Monte Carlo calculations.)

Note that in the central regions of the phantom, on the order of 50 percent of the dose is from photons which have suffered no prior collisions in the phantom (sum of DB-DB and AS-DB). The analytic calculation of the dose from these non-phantom-scattered photons should be essentially exact; hence, the 8 percent difference in the total dose fractions noted above may be attributed to the scattered component alone. This corresponds to an overestimate of approximately 16 percent in the scattered component of the analytic calculations.

In the analytic results it may be presumed that the absence of fine structure near the upper and lower extremities is a consequence of using infinite medium buildup factors. The excellent agreement between the analytic and Monte Carlo radial distributions near the lateral surfaces is fortuitous; the analytic calculations underpredict the dose fraction in these positions, relative to the central positions, because they do not include reflection of photons from deeper within the phantom. (See Sec. 3.3).

Figure 9 shows the Monte Carlo calculated depth-dose distributions for the phantom exposed to 23.8-hr fallout. A smoothed curve approximation of the Monte Carlo results for 1.12-hr fallout is included for comparison. The 23.8-hr results tend to be slightly lower near the phantom surfaces and higher near the center than did those for the 1.12-hr fallout However, it must be concluded that within the statistical accuracy of the results, the two ages of fallout produce essentially identical depth-dose distributions in the phantom. This conclusion is supported by the analytic

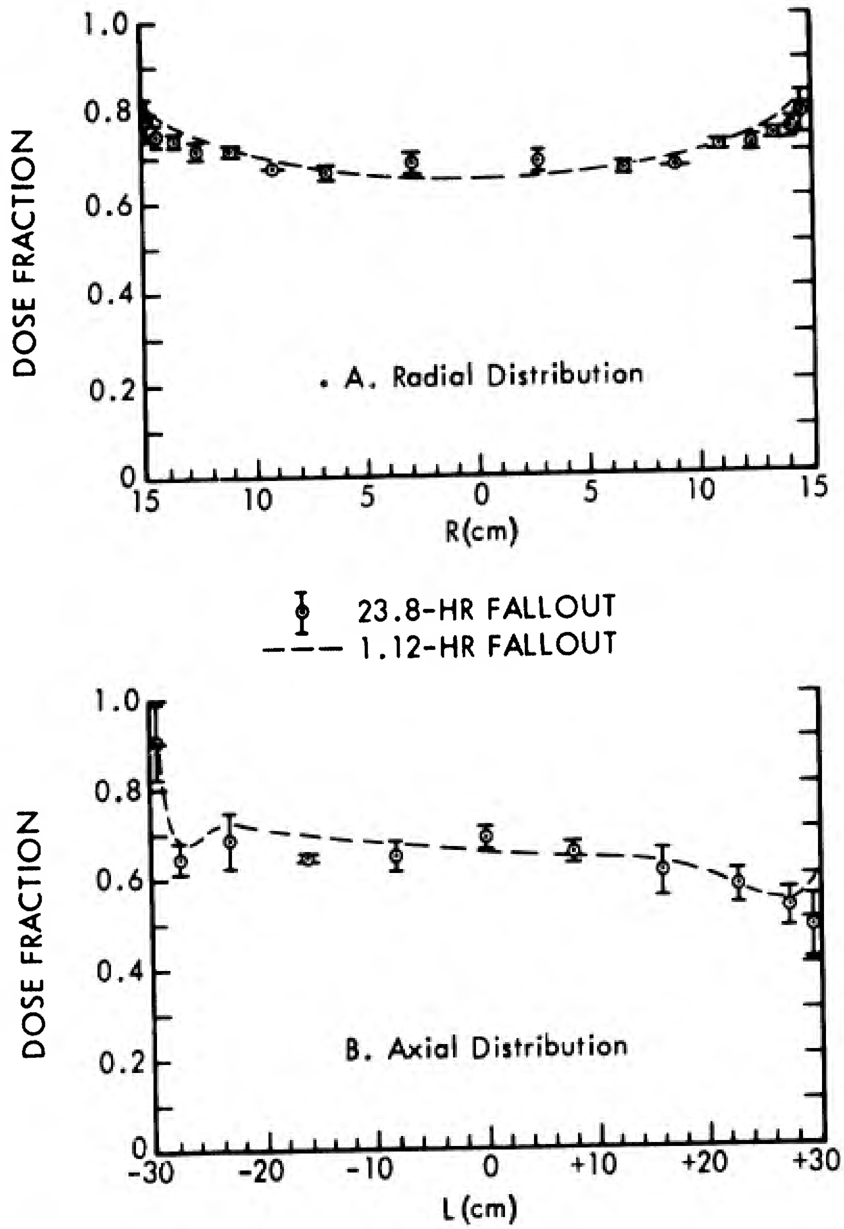

Figure 9. Comparison of Depth-Dose Distributions for 23.8-Hr and 1.12-Hr Fallout

results (see Table V) which differed by not more than 2 percent at any point in the phantom from those computed for 1.12-hr fallout.

Originally it was planned to perform Monte Carlo calculations for two additional ages of fallout; 4.57 and 9.82 days. These ages were not included in the Monte Carlo calculations because their energy spectra do not differ from that of 1.12-hr fallout as much as does that of 23.8-hr fallout, which was found to produce essentially the same depth-dose distributions as 1.12-hr fallout. Moreover, the analytic calculations performed for the two additional ages of fallout given in Table V are within approximately 1 percent of those for the earlier ages.

The Monte Carlo depth-dose distributions for a 1.12-hr fallout field as simulated by the AFRRI Compact Simulator are compared with those from 1.12-hr fallout in Figure 10. The radial distribution for the simulator is similar to that for the actual 1.12-hr fallout. The axial distribution is also similar but is slightly lower than that from the fallout. The depth-dose distributions for the AFRRI Compact Simulator computed with the simple analytic method are within 2 percent of the analytic results for the 1.12-hr fallout.

Figure 11 compares the Monte Carlo depth-dose distributions for the ^{60}Co point source at a horizontal separation distance of 200 ft (61 m) from the phantom with those produced by 1.12-hr fallout. The radial distribution for the ^{60}Co point source agrees very well in both shape and magnitude with that from the fallout. The axial distribution for the ^{60}Co is also similar to that from the fallout for $-20<L<+20$ cm. The ^{60}Co dose fraction is lower near the bottom of the phantom because the bottom surface is not exposed to a strong uncollided component as is the case with fallout. However, this difference is probably not of large significance since the cylindrical phantom itself is not representative of man near the axial extremities. Analytic calculation for the ^{60}Co agreed with the Monte

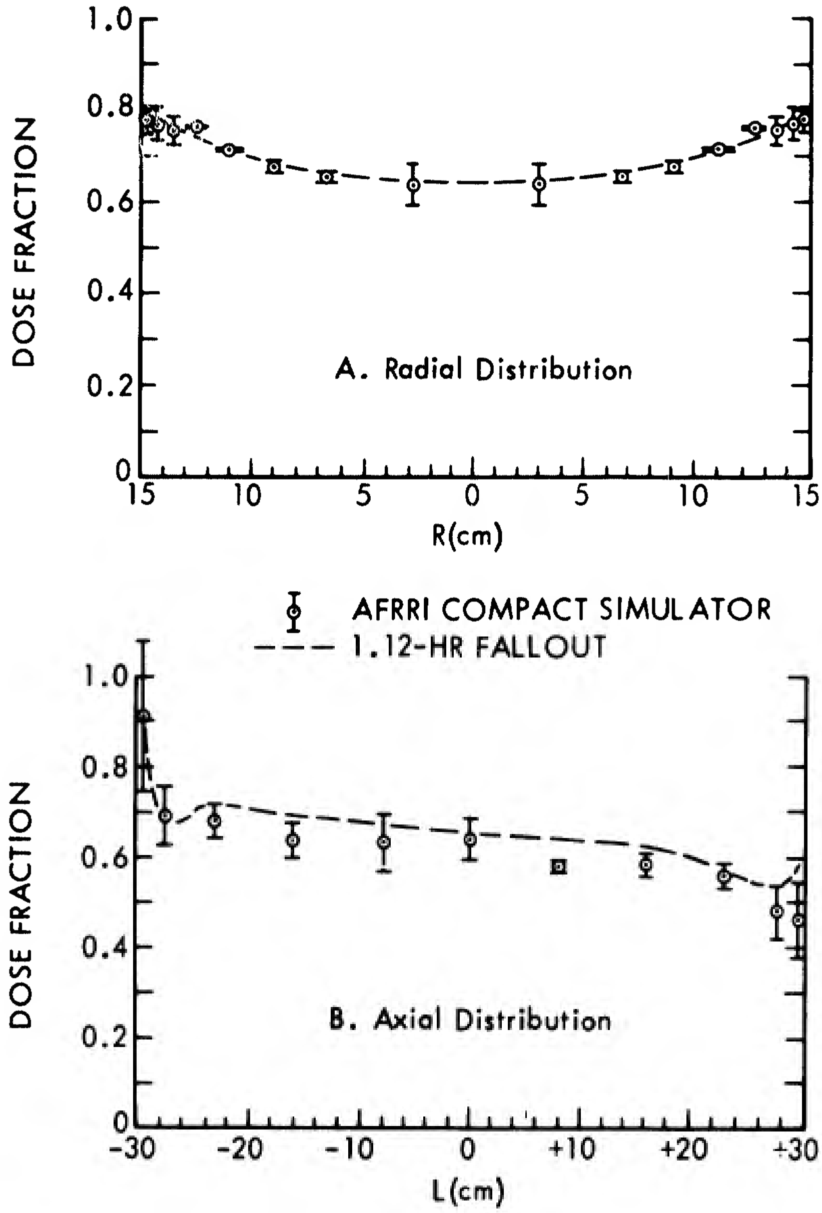

Figure 10. Comparison of Depth-Dose Distributions for AFRRI Compact Simulator and 1.12-Hr Fallout

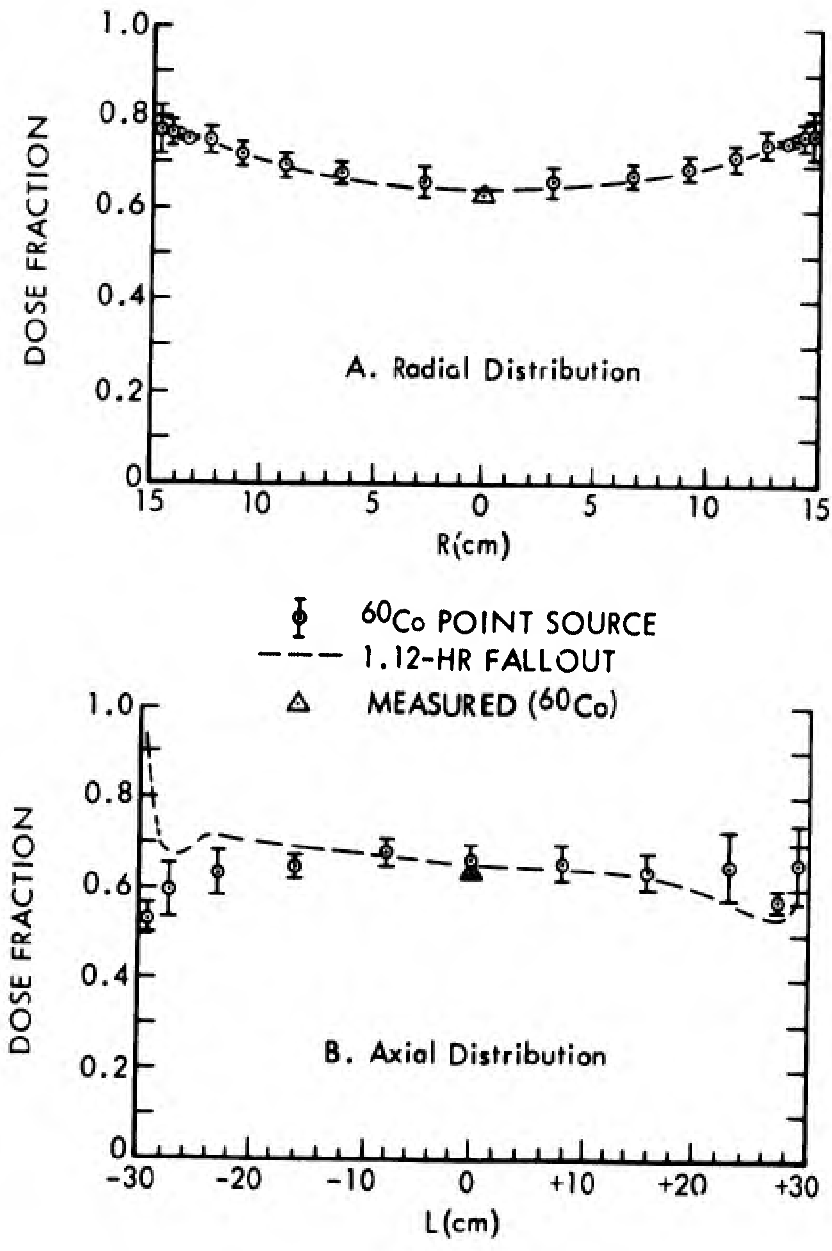

Figure 11. Comparison of Depth-Dose Distributions for ^{60}Co Point Source and 1.12-Hr Fallout

Carlo calculations to about the same extent as they did for the other sources.

Included in Figure 11 is the dose fraction measured by Menkes[28] at the center of a phantom for unilateral exposure to a ^{60}Co source at a horizontal distance of 60 m (~197 ft). Menkes' phantom was constructed of masonite (density = 1.00 ±0.02 gm/cm^3) and had a diameter of 30.5 cm and length of 66 cm as compared to the diameter of 30 cm and length of 60 cm for the phantom assumed in the present study. Although some difference between the calculated and measured dose fraction could be expected because of the minor differences in phantom dimensions, composition and density, the two agree within the standard deviation of the calculated value. Menkes measured dose fractions for other positions in the phantom but, because of the unilateral exposure used in the experiment, a valid comparison can be made with the Monte Carlo results only for the center position.

The depth-dose distributions computed by Monte Carlo for the phantom positioned at the center of the 4-ft diameter by 5-ft deep foxhole located in a 1.12-hr fallout field are compared with the distributions for the above ground 1.12-hr fallout case in Figure 12. No analytic calculations were performed for the foxhole. It is seen that the radial distribution is quite similar in shape to the above-ground case, with the greatest difference being the sharper drop-off of the dose away from the lateral surface. This is to be expected as the incident radiation in the foxhole is significantly softer than that above the ground.

As would also be expected, the axial distribution is completely different from that found above the ground. There is a significant drop-off in the total flux density from the top to the bottom of the foxhole. This, coupled with the fact that photons reaching the lower region of the foxhole have suffered a considerable number of collisions and therefore have a lower average energy, causes a

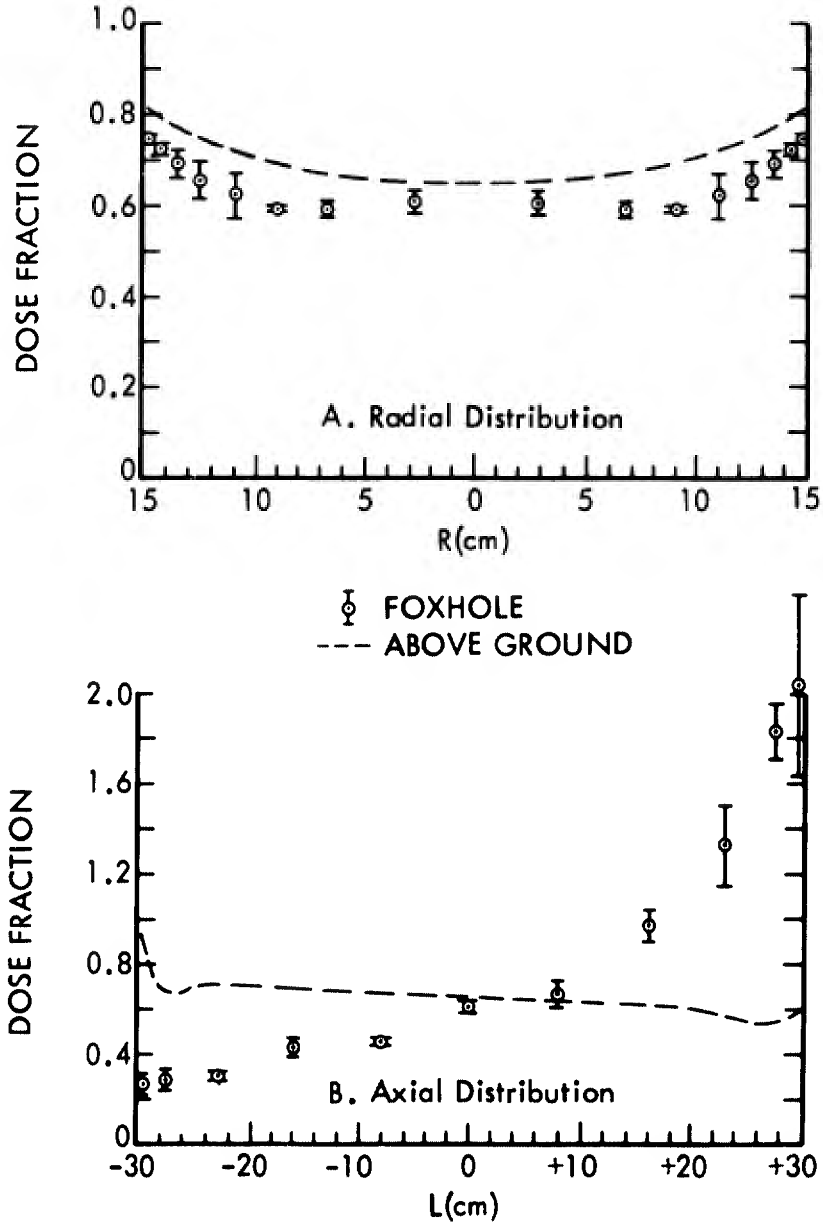

Figure 12. Comparison of Depth-Dose Distributions for Phantom in Foxhole and Above Ground (1.12-hr fallout)

decrease of an order of magnitude in the dose from the top of the phantom to the bottom.

It should be recalled that the ordinate scale on Figure 12 is the ratio of the dose in a phantom volume region to the free-field dose at the center of the foxhole. Since the upper part of the phantom was in a significantly higher incident flux density region, ratios above one were obtained.

4.2 Differential Energy Distribution of Absorbed Dose

The above-ground comparisons indicated that the depth-dose distributions from fallout are simulated reasonably well (except near the axial extremities) by both the AFRRI Compact Simulator and by the ^{60}Co point source. Also obtained were the energy distributions of the dose deposited in the phantom by the different sources.

Figure 13 compares the differential energy spectrum of the dose fraction at the center of the phantom based on the Monte Carlo calculations for the 1.12-hr fallout, the AFRRI Compact Simulator, the ^{60}Co point source, and the foxhole case. The dose energy spectra of the two simulators are both vastly different from that produced by fallout at energies above 1 MeV, and they show only a gross similarity below 1 MeV. The dose energy spectrum at the center of the phantom located in a foxhole resembles that for the above-ground 1.12-hr fallout case more closely than it does that for the simulated fallout. However, the lower energy photons contribute a much longer portion of the dose in the foxhole than above ground. The hump in the vicinity of 2 MeV is from the fallout gamma rays which penetrate directly through the "lip" of the foxhole.

The energy spectrum can be expected to vary with position in the phantom. Figure 14 compares the differential energy distribution of the Monte Carlo dose fractions at the top, center, bottom and side of the phantom exposed to 1.12-hr fallout with the differential energy distribution of the free-field dose. It is noted that the

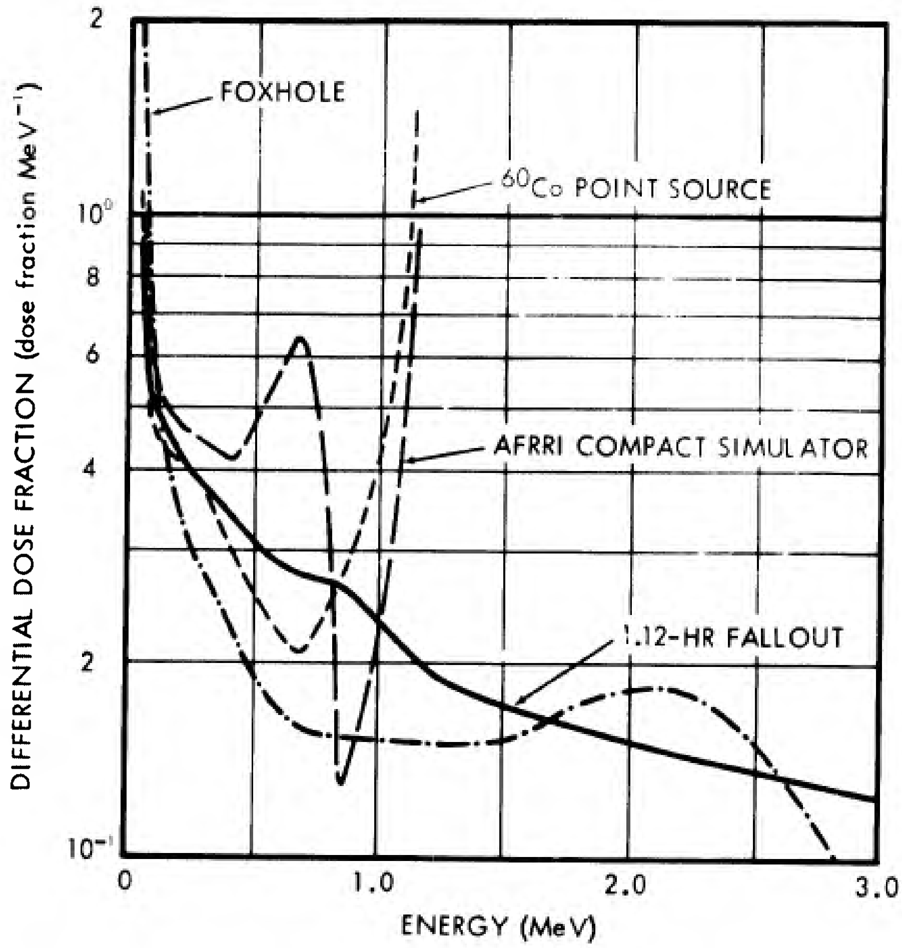

Figure 13. Differential Energy Distribution of Dose at Center of Phantom for Various Sources

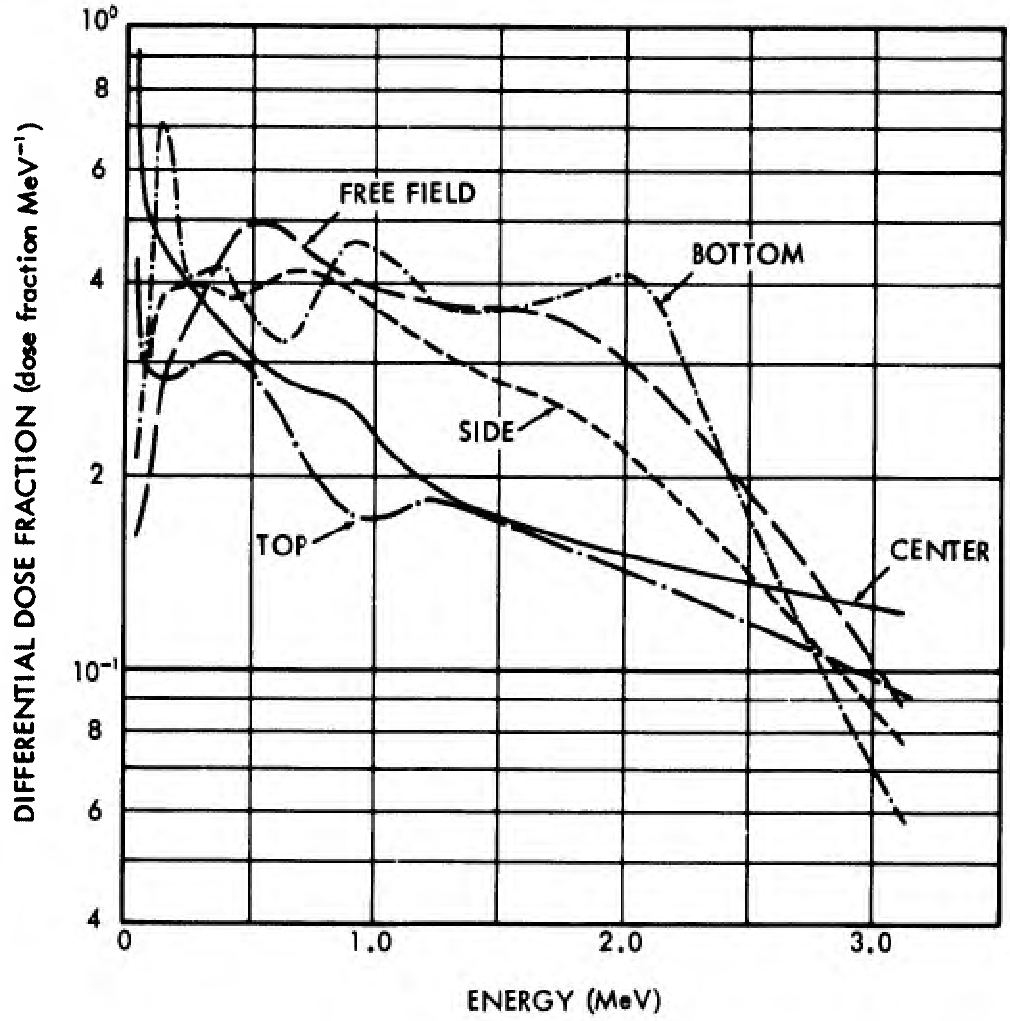

Figure 14. Differential Energy Distribution of Dose at Various Positions in Phantom for 1.12-Hr Fallout

distribution at the bottom and side resembles the free-field distribution more closely than does the distribution at the top and at the center. This is typical of the variation observed in the other radiation fields.

Another quantity obtained from the Monte Carlo results is the fraction of the total incident gamma-ray energy absorbed in the phantom exposed to each of the various radiation fields. This quantity is the sum of the energy deposited at all points in the phantom divided by the total energy incident on phantom surfaces. The results for the above-ground cases are given in Table VII.

Table VII. Fraction of Incident Energy Absorbed in Phantom for Various Sources

Source	Absorbed Energy Fraction
1.12-hr Fallout	0.4600±0.0011
23.8-hr Fallout	0.4854±0.0043
AFRRI Compact Simulator	0.5176±0.0012
^{60}Co Point Source	0.4876±0.0011

These fractions may, in a sense, be regarded as a measure of the "quality" of the radiation field. It is noted that the 1.12-hr fallout field deposits relatively less energy and that the AFRRI Compact Simulator deposits relatively more energy than the other sources.

4.3 Ground Roughness Effects

Exploratory calculations were performed to determine the sensitivity of the depth-dose patterns in the phantom to ground roughness effects since ground roughness can alter the energy and angle distribution of the gamma-ray flux density above fallout.[26] The calculations were performed for the uncollided component incident upon the phantom using the RRA-57 program which incorporates the buried source technique for simulating ground roughness effects. The calculations were performed for source energies of 0.67 and 1.25 MeV and for several source depths ranging from zero (smooth ground) to two inches (very rough ground).

Figure 15 shows the results of the ground roughness calculations for the 1.25-MeV source at depths of zero and two inches expressed as the fraction of the free-field dose rate from uncollided photons for corresponding source depths. The results for intermediate source depths fall between the two extremes shown in Figure 15. The largest change in the shape of the depth-dose curves as the source depth (or ground roughness) is increased occurs in the axial distribution near the bottom of the phantom ($-30<L<-20$ cm). The principal change in the radial distribution is a reduction of the dose fraction near the center. These changes are caused by alterations in the angle distribution of the photons incident upon the phantom. The results for the 0.67-MeV source were similar, although the change in slope near the bottom of the phantom as the source depth was increased was a little more pronounced.

From this cursory study of the ground roughness effect on the dose from the incident uncollided photons and the fact that the depth-dose distributions shown in the previous sections do not show a strong sensitivity to the energy and angle distributions of the incident radiation, it may be tentatively concluded that ground roughness is probably not an important factor in determining the depth-dose from fallout. Thus, the Monte Carlo calculations performed using the radiation environment above fallout on an idealized smooth ground surface are probably valid for real fallout deposited on actual ground whose surface has some degree of roughness.

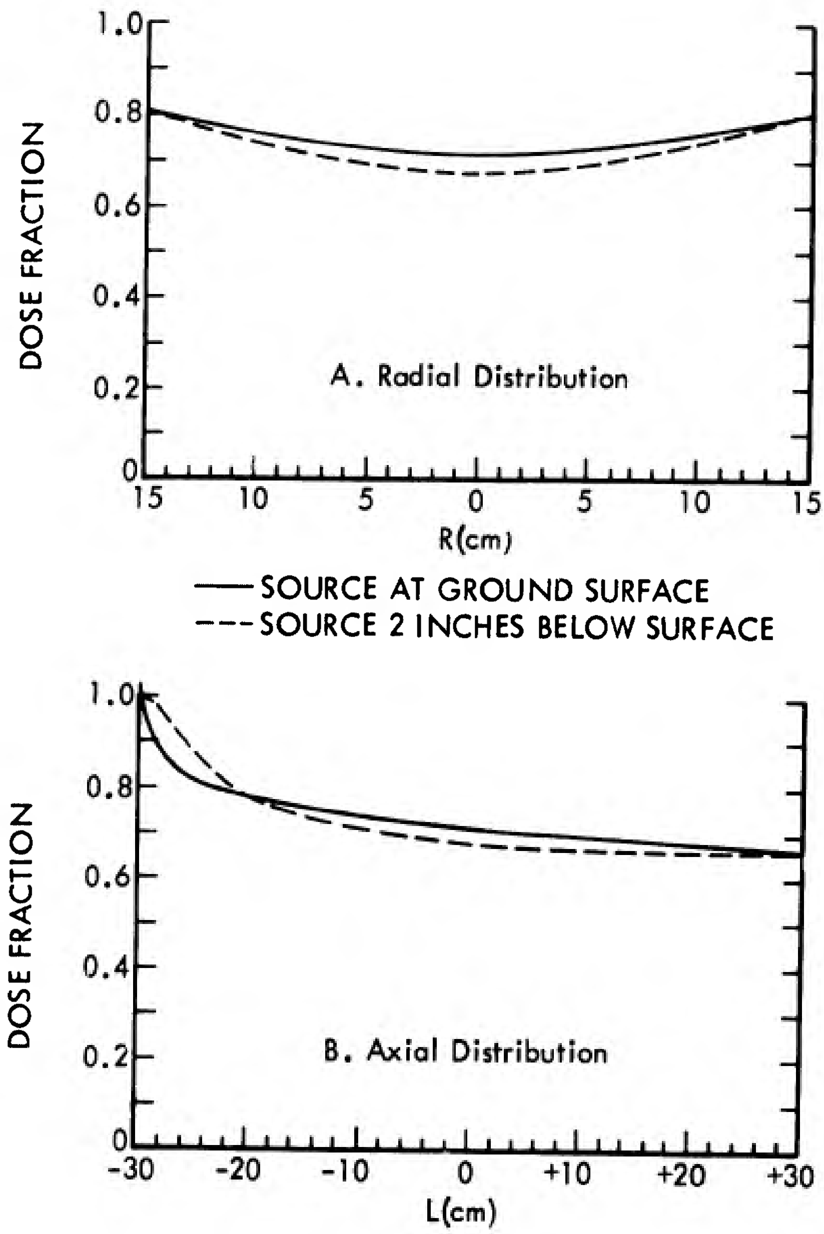

Figure 15. Effect of Ground Roughness on the Depth-Dose Distribution from the Uncollided Component incident upon Phantom Exposed to 1.25-MeV Infinite Plane Source

V. CONCLUSIONS

From the results of this study, several significant conclusions can be drawn and, as often is the case, several important and unanswered questions have been brought into focus. The study was successful in that all of the objectives set forth at the beginning of the effort were attained. The methods used proved adequate for this task and the desired results were obtained with sufficient accuracy to enable valid comparisons of the depth-dose patterns between the various geometries considered.

One of the most striking observations that can be made is the insensitivity of the depth-dose pattern to variations in the incident photon angle and energy distribution. The insensitivity to source energy spectra is exhibited in the essentially identical depth-dose distributions for all four ages of fallout and the AFRRI Compact Simulator, even though the latter lacks the high energy photons (>1.33 MeV) present in fallout. Although the incident angle distribution was quite different, the axial distribution of the ^{60}Co point source simulator showed only a minor variation from the other above-ground cases and the radial dose profile was identical to them.

The incident photon distributions for the foxhole are very dissimilar to the others, yet major variations in the dose patterns were exhibited only in the axial direction. Further, the exploratory calculations performed to evaluate ground roughness effects on the depth-dose distributions displayed the same insensitivity. It may be safely concluded that the scattering and absorbing properties and the size of the phantom reduce the effects of differences in the free-field properties, and that rather large changes in the incident photon angle and energy distributions cause smaller changes in the depth-dose patterns.

Both fallout simulators produced depth-dose patterns that were very similar to those computed for actual fallout and either would appear to be appropriate simulation devices from this standpoint. However, the dose spectrum in each simulator does differ from that of fallout due to the absence of the higher energy photons present in quantity in fallout. A question left unanswered by this study is whether this difference in dose spectra would compromise the use of the simulator for biological studies.

Perforce, the model used in these studies for the actual fallout field was highly idealized. Whereas the effect of ground roughness on the results was explored, other possible effects such as a nonuniform fallout deposition, macroscopic terrain features, foliage, structures, etc. which could affect the depth-dose distributions, were not investigated. The insensitivity of the dose profiles to the free-field characteristics would indicate that such effects may not be large; however, such conclusions must await the results of further investigation.

Regarding the methods employed to calculate these depth-dose distributions, the Monte Carlo technique appears to work well. Although the foxhole calculations presented special problems, sufficient accuracy for the purposes of the study was attained with the expenditure of a reasonable amount of computer time for both the above-ground and foxhole cases. Agreement with both the available experimental data and with the analytic calculations demonstrates the validity of the technique. Indeed, the more approximate but faster analytic calculations yielded results close enough to the Monte Carlo and experimental data to give that method merit for the simpler geometries when high precision is not required.

REFERENCES

1. R. L. Mather et al., Health Physics 8, 245 (1962).

2. C. M. Huddleston et al., Health Physics 11, 537 (1965).

3. C. F. Ksanda et al., Gamma Radiation from a Rough Infinite Plane, Naval Radiological Defense Laboratory Report USNRDL-TR-108 (1956).

4. R. L. Rexroad and M. A. Schmoke, Scattered Radiation and Free Field Dose Rates from Distributed Cobalt-60 and Cesium-137 Sources, Nuclear Defense Laboratory Report NDL-TR-2 (1960).

5. C. L. Schlemn et al., Scattered Gamma Radiation Measurements from a ^{60}Co Contaminated Field, Air Force Special Weapons Center Report AFSWC-TN-59-6 (1959).

6. F. J. Davis and P. W. Reinhardt, Health Physics 8, 233 (1962).

7. Z. G. Burson et al., Description and Operating Instructions for the Mobile Radiological Measuring Unit (MRMU), Edgerton, Germeshausen and Grier, Inc. Report L-608 (1963).

8. E. T. Clarke et al., Measurements of Attenuation in Existing Structures of Radiation from Simulated Fallout, Technical Operations, Inc. Report TO-B-59-4 (1959).

9. C. K. Menkes and C. K. Tochilin, Radiology 82, 128 (1964).

10. R. L. Rexroad et al., A Point-Source Circulation System for Simulating Fallout Gamma Radiation, Nuclear Defense Laboratory Report NDL-TM-15 (1964).

11. C. McDonnell et al., Description, Experimental Calibration and Analysis of the Radiation Test Facility at the Protective Structures Development Center, Protective Structures Development Center Report PSDC-TR-14 (1964).

12. T. H. M. Crampton et al., Development of a Fallout Simulator, Armed Forces Radiobiology Research Institute Report 1-63 (1963).

13. W. Lee and H. Borella, Methods and Techniques of Fallout Studies Using a Particulate Simulant, Edgerton, Germeshausen and Grier, Inc. Report CEX-59.7C (1962).

14. L. V. Spencer, Structure Shielding Against Fallout Radiation from Nuclear Weapons, National Bureau of Standards Monograph 42 (1962).

15. G. W. Imirie, Jr. and R. Sharp, Radiation Energy Absorbed by Human Phantoms in a Fission Fallout Field, Armed Forces Special Weapons Project Report WT-1120 (1955).

16. V. P. Bond *et al.*, Radiation Research *6*, 554 (1957).

17. R. L. French, Health Physics *11*, 369 (1965).

18. R. L. French, A Comparative Study of Radioactive Source Arrangements for Simulating Fallout Gamma Radiation Fields, Armed Forces Radiobiology Research Institute Report CR 65-2 (1965) originally published as Radiation Research Associates Report RRA-T45 (1964).

19. A. T. Nelms and T. W. Cooper, Health Physics *1*, 427 (1959).

20. G. W. Grodstein, X-ray Attenuation Coefficients from 10 KeV to 100 MeV, National Bureau of Standards Circular 583 (1957).

21. D. G. Collins, Utilization Instructions for General Application of the L05 Monte Carlo Procedure, Armed Forces Radiobiology Research Institute Report CR 65-1 (1965) originally published as Radiation Research Associates Report RRA-T44 (1964).

22. M. B. Wells and C. F. Malone, A Monte Carlo Procedure for Radiation Transport and Heating Studies, Nuclear Aerospace Research Facility Report FZK-156 (1962).

23. D. G. Collins and M. B. Wells, COHORT, a Monte Carlo Program for Calculation of Radiation Heating and Transport, Vols. I-IV, Radiation Research Associates Report RRA-T62 (1966).

24. J. H. Price, RRA-62, A Special Version of the COHORT S01 Code, Armed Forces Radiobiology Research Institute Report CR 67-2, prepared as RRA-T72 by Radiation Research Associates (1967).

25. B. J. Henderson, Conversion of Neutron or Gamma Ray Flux to Absorbed Dose Rate, General Electric Report XDC 59-8-179 (1959).

26. R. L. French and L. Olmedo, Ground Roughness Calculations for Fallout Gamma Rays, Radiation Research Associates Report RRA-T61 (1966).

27. H. Goldstein and J. E. Wilkins, Jr., Calculations of the Penetration of Gamma Rays, NYO-3075 (1954).

28. C. W. Menkes, Health Physics *12*, 1115 (1966).

APPENDIX

Free-Field Gamma-Ray Energy and Angle Distributions Used for Depth-Dose Calculations

---

Note: Read 1.197E-08 or 1.197-08 as 1.197×10^{-8}.
ANG indicates upper bound of 10-degree interval on θ.
ENG indicates upper bound of energy interval (MeV).

Table A1. Energy and Angle Distribution of the Photon Number Flux Density 3 ft above 1.12-hr Fallout Consisting of the Products of one ^{235}U Fission per cm^2 of Ground Surface

(photons/cm^2-sec)

ANG/ENG	0.060	0.100	0.180	0.300	0.500	0.750	1.000	1.500	2.500	3.000	SUM	DOSE RATE
10	1.197E-08	6.967E-08	1.436E-07	2.001E-07	1.826E-07	1.292E-07	8.266E-08	1.083E-07	1.794E-07	3.230E-08	1.090E-06	1.276E-12
20	3.747E-08	2.666E-07	5.847E-07	5.959E-07	5.617E-07	4.074E-07	2.528E-07	3.313E-07	3.958E-07	9.886E-08	3.533E-06	3.928E-12
30	6.088E-08	4.508E-07	9.597E-07	9.404E-07	1.179E-06	8.124E-07	4.399E-07	5.763E-07	6.888E-07	1.720E-07	6.280E-06	7.026E-12
40	7.704E-08	6.490E-07	1.306E-06	1.326E-06	1.297E-06	1.141E-06	6.602E-07	8.653E-07	1.034E-06	2.583E-07	8.615E-06	1.010E-11
50	5.569E-08	5.783E-07	1.581E-06	1.736E-06	1.933E-06	1.688E-06	1.002E-06	1.236E-06	1.477E-06	3.691E-07	1.166E-05	1.448E-11
60	1.449E-07	9.620E-07	1.883E-06	2.085E-06	2.649E-06	2.250E-06	1.467E-06	1.782E-06	2.126E-06	5.279E-07	1.588E-05	2.029E-11
70	1.218E-07	1.190E-06	2.772E-06	3.098E-06	4.607E-06	3.750E-06	2.219E-06	2.886E-06	3.216E-06	7.957E-07	2.466E-05	3.186E-11
80	1.610E-07	1.237E-06	3.552E-06	4.166E-06	7.653E-06	6.759E-06	3.992E-06	5.056E-06	5.676E-06	1.412E-06	3.966E-05	5.518E-11
90	6.056E-07	1.839E-06	7.867E-06	9.381E-06	2.235E-05	2.254E-05	1.444E-05	2.031E-05	2.526E-05	6.930E-06	1.315E-04	2.151E-10
100	5.782E-07	2.966E-06	4.098E-06	3.683E-06	2.612E-06	1.356E-06	9.790E-07	1.900E-06	2.135E-07	1.523E-07	1.054E-05	1.286E-11
110	8.910E-07	2.023E-06	2.969E-06	3.315E-06	1.550E-06	9.615E-07	2.285E-08	1.558E-07	4.801E-08	0.	1.194E-05	5.036E-1[illegible]
120	7.181E-07	2.917E-06	2.859E-06	2.023E-06	8.139E-07	1.466E-07	1.882E-07	0.	0.	0.	9.665E-06	3.065E-12
130	1.111E-06	2.026E-06	2.106E-06	1.011E-06	8.660E-07	1.309E-07	0.	0.	0.	0.	7.250E-06	2.095E-12
140	1.675E-06	1.852E-06	1.532E-06	1.418E-06	1.205E-07	1.191E-08	0.	0.	0.	0.	6.609E-06	1.472E-1[illegible]
150	4.815E-07	1.012E-06	7.471E-07	6.642E-07	1.562E-07	1.535E-08	0.	0.	0.	0.	3.077E-06	7.360E-13
160	7.483E-07	1.643E-06	1.022E-06	5.973E-07	7.799E-08	2.623E-09	0.	0.	0.	0.	4.091E-06	8.079E-13
170	3.425E-07	7.226E-07	3.820E-07	2.899E-07	2.216E-09	1.929E-09	0.	0.	0.	0.	1.741E-06	3.390E-13
180	1.455E-07	8.012E-07	1.892E-07	2.822E-08	1.413E-08	8.526E-10	0.	0.	0.	0.	1.179E-06	2.038E-13
SUM	7.967E-06	2.321E-05	3.655E-05	3.655E-05	4.863E-05	4.210E-05	2.575E-05	3.521E-05	4.027E-05	1.075E-05	3.070E-04	3.859E-10

Table A2. Energy and Angle Distribution of the Photon Number Flux Density 3 ft above 23.8-hr Fallout Consisting of the Products of one ^{235}U Fission per cm^2 of Ground Surface

(photons/cm^2-sec)

ANG/ENG	0.060	0.100	0.180	0.300	0.500	0.750	1.000	1.500	2.500	3.500	SUM	DOSE RATE
10	2.361E-10	1.614E-09	2.830E-09	5.278E-09	1.718E-09	4.358E-09	5.181E-09	1.013E-09	5.724E-10	6.867E-12	2.281E-08	2.141E-14
20	8.244E-10	5.296E-09	1.232E-08	1.522E-08	7.582E-09	1.341E-08	1.585E-08	3.099E-09	1.751E-09	2.101E-11	7.538E-08	6.712E-14
30	1.234E-09	1.064E-08	2.255E-08	2.343E-08	1.391E-08	2.492E-08	2.758E-08	5.390E-09	3.047E-09	3.656E-11	1.327E-07	1.184E-13
40	1.323E-09	1.121E-08	2.680E-08	3.445E-08	1.565E-08	3.533E-08	4.139E-08	8.093E-09	4.574E-09	5.491E-11	1.789E-07	1.695E-13
50	1.339E-09	1.246E-08	3.182E-08	4.619E-08	2.326E-08	5.109E-08	5.927E-08	1.156E-08	6.534E-09	7.846E-11	2.436E-07	2.401E-13
60	4.088E-09	2.082E-08	4.407E-08	5.887E-08	3.411E-08	7.527E-08	3.513E-08	1.652E-08	9.359E-09	1.122E-10	3.484E-07	3.442E-13
70	3.296E-09	2.530E-08	5.790E-08	8.314E-08	6.912E-08	1.224E-07	1.280E-07	2.561E-08	1.411E-08	1.691E-10	5.290E-07	5.380E-13
80	6.517E-09	3.466E-08	7.136E-08	1.196E-07	1.055E-07	2.202E-07	2.267E-07	4.531E-08	2.491E-08	3.001E-10	8.551E-07	9.254E-13
90	1.688E-08	4.097E-09	1.642E-07	2.826E-07	3.093E-07	7.670E-07	8.729E-07	1.869E-07	1.096E-07	1.473E-09	2.752E-06	3.351E-12
100	1.149E-08	6.559E-08	7.580E-08	7.571E-08	6.915E-08	3.733E-08	2.670E-08	1.574E-08	2.273E-10	3.237E-11	3.777E-07	2.242E-13
110	2.054E-08	4.146E-08	5.147E-08	6.387E-08	3.682E-08	3.495E-08	1.176E-10	3.375E-10	1.021E-11	0.	2.496E-07	1.129E-13
120	1.743E-08	5.719E-08	8.977E-08	3.765E-08	1.951E-08	1.300E-09	6.279E-10	0.	0.	0.	2.034E-07	6.156E-14
130	2.6[illegible]7E-08	4.771E-08	4.352E-08	2.114E-08	2.514E-08	9.814E-10	0.	0.	0.	0.	1.646E-07	4.833E-14
140	7.552E-08	3.569E-08	3.297E-08	3.779E-08	4.301E-10	1.884E-11	0.	0.	0.	0.	1.823E-07	3.900E-14
150	1.456E-08	2.012E-08	1.690E-08	1.152E-08	5.645E-09	9.673E-12	0.	0.	0.	0.	6.875E-08	1.611E-14
160	1.376E-08	5.217E-08	2.674E-08	1.846E-08	3.406E-10	4.297E-12	0.	0.	0.	0.	1.115E-07	2.089E-14
170	9.767E-09	1.300E-08	1.006E-08	8.905E-09	5.280E-13	1.346E-12	0.	0.	0.	0.	4.174E-08	8.731E-15
180	2.092E-09	9.647E-09	3.253E-09	5.389E-10	7.253E-11	2.970E-12	0.	0.	0.	0.	1.560E-08	2.748E-15
SUM	2.270E-07	5.056E-07	7.642E-07	9.443E-07	7.375E-07	1.388E-06	1.490E-06	3.196E-07	1.747E-07	2.284E-09	6.553E-06	6.310E-12

Table A3. Energy and Angle Distribution of the Photon Number Flux Density 3 ft above 4.57-day Fallout Consisting of the Products of one ^{235}U Fission per cm^2 of Ground Surface

(photons/cm^2-sec)

ANG/ENG	0.060	0.100	0.180	0.300	0.500	0.750	1.000	1.500	2.500	3.500	SUM	DOSE RATE
10	3.409E-11	2.919E-10	6.402E-10	7.353E-10	3.478E-10	2.769E-10	2.953E-10	9.869E-11	1.926E-10	8.584E-12	2.921E-09	2.304E-15
20	1.333E-10	1.101E-09	2.384E-09	2.184E-09	1.121E-09	8.561E-10	9.034E-10	3.020E-10	5.892E-10	2.627E-11	9.601E-09	7.155E-15
30	2.807E-10	1.796E-09	3.787E-09	3.731E-09	2.338E-09	1.704E-09	1.572E-09	5.253E-10	1.025E-09	4.570F-11	1.672E-08	1.281E-14
40	2.644E-10	2.543E-09	5.709E-09	5.408E-09	2.614E-09	2.353E-09	2.359E-09	7.886E-10	1.539E-09	6.863E-11	2.365E-08	1.834E-14
50	2.098E-10	2.366E-09	6.982E-09	7.671E-09	3.823E-09	3.421E-09	3.435E-09	1.126E-09	2.199E-09	9.807E-11	3.133E-08	2.593E-14
60	4.722E-10	3.625E-09	9.091E-09	9.885E-09	5.470E-09	4.826E-09	4.937E-09	1.614E-09	3.145E-09	1.403E-10	4.3216-08	3.645E-14
70	5.342E-10	4.510E-09	1.320E-08	1.560E-08	9.607E-09	7.941E-09	7.449E-09	2.686E-09	4.739E-09	2.114E-10	6.648E-08	5.726E-14
80	6.372E-10	5.864E-09	1.807E-08	2.411E-08	1.605E-08	1.430E-08	1.321E-08	4.779E-09	8.380E-09	3.751E-10	1.058E-07	9.828E-14
90	1.750E-09	1.071E-08	4.975E-08	7.027E-08	4.850E-08	4.880E-08	5.032E-08	1.886E-08	3.677E-08	1.841E-09	3.376E-07	3.597E-13
100	2.082E-09	1.097E-08	1.336E-08	1.075E-08	5.802E-09	2.943E-09	2.009E-09	2.065E-09	4.821E-11	4.046E-11	5.006E-08	2.402E-14
110	3.325E-09	6.639E-09	8.759E-09	9.169E-09	3.229E-09	2.280E-09	4.124E-11	1.327E-10	1.276E-11	0.	3.359E-08	1.216E-14
120	3.501E-09	8.105E-09	1.147E-08	3.981E-09	1.653E-09	2.154E-10	2.334E-10	0.	0.	0.	2.916E-08	7.579E-15
130	3.259E-09	8.754E-09	7.796E-09	1.934E-09	1.724E-09	1.379E-10	0.	0.	0.	0.	2.360E-08	5.491E-15
140	6.256E-09	7.421E-09	4.391E-09	3.099E-09	1.476E-10	7.106E-12	0.	0.	0.	0.	2.132E-08	4.108E-15
150	1.757E-09	4.091E-09	2.738E-09	1.465E-09	4.032E-10	5.677E-12	0.	0.	0.	0.	1.046E-08	2.161E-15
160	3.129E-09	6.382E-09	4.350E-09	1.314E-09	1.212E-10	1.729E-12	0.	0.	0.	0.	1.530E-08	2.705E-15
170	2.354E-09	2.033E-09	2.030E-09	6.740E-10	5.844E-13	7.734E-13	0.	0.	0.	0.	7.092E-09	1.262E-15
180	3.542E-10	1.888E-09	3.535E-10	4.963E-11	2.542E-11	1.078E-12	0.	0.	0.	0.	2.677E-09	4.445E-16
SUM	3.025E-08	8.910E-08	1.649E-07	1.720E-07	1.030E-07	9.006E-08	8.678E-08	3.297E-08	5.866E-08	2.855E-09	8.305E-07	6.782E-13

Table A4. Energy and Angle Distribution of the Photon Number Flux Density 3 ft above 9.82-day Fallout Consisting of the Products of one ^{235}U Fission per cm^2 of Ground Surface

(photons/cm^2-sec)

ANG/ENG	0.060	0.100	0.180	0.300	0.500	0.750	1.000	1.500	2.500	3.500	SUM	DOSE RATE
10	1.620E-11	1.489E-10	3.096E-10	3.040E-10	1.687E-10	1.285E-10	1.426E-10	2.281E-11	1.721E-10	7.897E-12	1.421E-09	1.256E-15
20	6.460E-11	5.456E-10	1.116E-09	9.013E-10	5.062E-10	3.960E-10	4.361E-10	6.981E-11	5.264E-10	2.416E-11	4.586E-09	3.857E-15
30	1.045E-10	8.992E-10	1.810E-09	1.545E-09	1.255E-09	8.536E-10	7.588E-10	1.214E-10	9.161E-10	4.204E-11	8.306E-09	7.082E-15
40	1.263E-10	1.264E-09	2.634E-09	2.136E-09	1.161E-09	1.141E-09	1.139E-09	1.823E-10	1.375E-09	6.314E-11	1.122E-08	9.911E-15
50	1.099E-10	1.249E-09	3.413E-09	3.049E-09	1.700E-09	1.641E-09	1.686E-09	2.604E-10	1.965E-09	9.022E-11	1.517E-08	1.413E-14
60	2.234E-10	1.802E-09	4.364E-09	3.841E-09	2.452E-09	2.266E-09	2.399E-09	3.761E-10	2.810E-09	1.290E-10	2.066E-08	1.979E-14
70	2.388E-10	2.334E-09	6.494E-09	5.990E-09	4.282E-09	3.750E-09	3.643E-09	7.961E-10	4.234E-09	1.945E-10	3.196E-08	3.116E-14
80	3.171E-10	3.129E-09	9.108E-09	8.994E-09	7.061E-09	6.755E-09	6.403E-09	1.441E-09	7.487E-09	3.450E-10	5.104E-08	5.370E-14
90	8.265E-10	5.701E-09	2.485E-08	2.496E-08	2.103E-08	2.271E-08	2.448E-08	4.952E-09	3.285E-08	1.694E-09	1.641E-07	2.017E-13
100	9.653E-10	5.199E-09	5.871E-09	4.493E-09	2.936E-09	1.705E-09	1.078E-09	9.673E-10	4.210E-11	3.722E-11	2.329E-08	1.192E-14
110	1.523E-09	3.122E-09	4.015E-09	4.053E-09	1.920E-09	1.132E-09	3.691E-11	1.193E-10	1.174E-11	0.	1.593E-08	6.089E-15
120	1.571E-09	3.853E-09	4.564E-09	2.035E-09	9.550E-10	1.597E-10	2.094E-10	0.	0.	0.	1.334E-08	3.819E-15
130	1.566E-09	4.112E-09	3.161E-09	1.118E-09	8.788E-10	7.124E-11	0.	0.	0.	0.	1.091E-08	2.611E-15
140	2.901E-09	3.615E-09	1.966E-09	1.540E-09	1.307E-10	6.377E-12	0.	0.	0.	0.	1.016E-08	2.007E-15
150	8.611E-10	1.818E-09	1.129E-09	6.997E-10	2.270E-10	5.161E-12	0.	0.	0.	0.	4.740E-09	1.014E-15
160	1.367E-09	2.762E-09	1.817E-09	6.997E-10	1.086E-10	1.555E-12	0.	0.	0.	0.	6.757E-09	1.247E-15
170	9.560E-10	8.595E-10	8.102E-10	3.333E-10	5.369E-13	7.026E-13	0.	0.	0.	0.	2.990E-09	5.408E-16
180	1.596E-10	8.243E-10	1.521E-10	2.876E-11	2.275E-11	9.661E-13	0.	0.	0.	0.	1.188E-09	2.044E-16
SUM	1.390E-08	4.327E-08	7.759E-08	6.672E-08	4.681E-08	4.273E-08	4.242E-08	9.309E-09	5.241E-08	2.627E-09	3.978E-07	3.721E-13

Table A5. Energy and Angle Distribution of the Scattered Photon Number Flux Density 3 ft above the Ground and 200 ft from a ^{60}Co Point Source also 3 ft above the Ground

(photons/cm^2-sec)

ANG/ENG	0.060	0.100	0.180	0.300	0.500	0.750	1.000	1.500	2.500	3.500	SUM	DOSE RATE
10	3.955E-14	1.342E-13	1.161E-13	3.125E-14	7.022E-14	0.	0.	0.	0.	0.	3.913E-13	1.057E-19
20	1.446E-13	4.434E-13	4.051E-13	1.936E-13	4.047E-13	0.	0.	0.	0.	0.	1.591E-12	5.204E-19
30	1.793E-13	6.419E-13	6.849E-13	5.496E-13	4.441E-13	0.	0.	0.	0.	0.	2.500E-12	8.469E-19
40	2.543E-13	1.040E-12	9.714E-13	4.740E-13	7.211E-13	4.139E-14	0.	0.	0.	0.	3.502E-12	1.231E-18
50	3.613E-13	1.362E-12	1.236E-12	1.098E-12	6.163E-13	7.951E-13	0.	0.	0.	0.	5.469E-12	2.276E-18
60	3.754E-13	2.033E-12	2.024E-12	2.045E-12	9.144E-13	2.379E-12	1.849E-14	0.	0.	0.	9.790E-12	4.843E-18
70	4.598E-11	1.397E-10	2.385E-12	2.733E-12	1.153E-12	4.815E-12	1.021E-13	6.369E-15	0.	0.	1.969E-10	3.128E-17
80	5.102E-13	2.299E-12	4.142E-12	6.060E-11	6.264E-12	9.815E-13	1.365E-11	2.379E-13	0.	0.	8.868E-11	5.565E-17
90	3.250E-11	1.446E-11	3.871E-11	3.536E-11	6.215E-11	1.804E-11	1.317E-11	7.518E-11	0.	0.	2.896E-10	2.668E-16
100	4.964E-11	4.947E-11	4.989E-11	4.367E-11	5.739E-11	3.438E-11	2.087E-11	2.464E-11	0.	0.	3.300E-10	2.106E-16
110	1.879E-11	3.692E-11	5.806E-11	4.040E-11	2.053E-11	1.421E-11	3.077E-11	0.	0.	0.	2.197E-10	1.157E-16
120	1.330E-11	1.430E-11	9.136E-11	4.642E-11	1.464E-11	1.102E-11	7.485E-12	0.	0.	0.	1.986E-10	7.858E-17
130	9.675E-12	3.948E-11	5.571E-11	2.297E-11	1.087E-11	1.584E-12	0.	0.	0.	0.	1.402E-10	3.750E-17
140	7.187E-12	3.268E-11	4.433E-11	1.586E-11	4.052E-12	0.	0.	0.	0.	0.	1.041E-10	2.408E-17
150	2.721E-11	3.962E-11	1.864E-11	1.040E-11	3.622E-12	1.112E-14	0.	0.	0.	0.	9.949E-11	2.037E-17
160	1.168E-11	7.783E-12	1.864E-11	6.524E-12	1.098E-11	0.	0.	0.	0.	0.	5.560E-11	1.578E-17
170	1.956E-12	4.643E-12	2.744E-12	4.324E-12	0.	0.	0.	0.	0.	0.	1.367E-11	3.360E-18
180	1.031E-12	3.116E-13	3.465E-13	9.925E-13	0.	0.	0.	0.	0.	0.	2.682E-12	6.244E-19
SUM	2.208E-10	3.874E-10	3.904E-10	2.947E-10	1.948E-10	8.826E-11	8.607E-11	1.001E-10	0.	0.	1.762E-09	8.698E-16

Table A6. Energy and Angle Distribution of the Photon Number Flux Density at the Center of the AFRRI Compact Simulator

(photons/cm^2-sec)

ANG/ENG	0.060	0.100	C.18C	0.300	0.500	0.750	1.00C	1.500	2.500	3.500	SUM	DOSE RATE
10	1.547E-08	1.801E-07	1.106E-07	1.311E-07	1.781E-08	3.412E-07	0.	2.716E-07	0.	0.	1.068E-06	1.107E-12
20	5.396E-08	5.451E-07	7.063E-07	5.512E-07	1.165E-07	1.050E-06	0.	8.309E-07	0.	0.	3.853E-06	3.564E-12
30	1.153E-07	9.028E-07	5.858E-07	8.546E-07	2.599E-07	1.821E-06	8.744E-09	1.445E-06	0.	0.	5.993E-06	6.075E-12
40	1.039E-07	1.586E-06	8.690E-07	1.104E-06	5.787E-07	2.777E-06	9.519E-09	2.170E-06	0.	0.	9.197E-06	9.280E-12
50	1.157E-07	1.666E-06	1.024E-06	1.323E-06	6.401E-07	4.025E-06	0.	3.099E-06	0.	0.	1.189E-05	1.292E-11
60	1.912E-07	2.623E-06	1.091E-06	1.530E-06	1.078E-06	5.819E-06	1.174E-07	4.429E-06	0.	0.	1.688E-05	1.863E-11
70	2.147E-07	3.791E-06	1.241E-06	2.151E-06	1.976E-06	9.036E-06	2.164E-07	6.717E-06	0.	0.	2.534E-05	2.867E-11
80	3.294E-07	4.842E-06	1.499E-06	2.392E-06	1.962E-06	1.620E-05	2.150E-07	1.255E-05	0.	0.	3.999E-05	4.973E-11
90	3.390E-07	1.123E-05	1.995E-06	2.683E-06	3.692E-06	5.863E-05	1.377E-06	5.035E-05	0.	0.	1.303E-04	1.851E-10
100	4.888E-07	2.043E-06	1.664E-06	2.539E-06	3.597E-06	3.506E-06	1.410E-06	9.238E-07	0.	C.	1.617E-05	1.248E-11
110	3.541E-07	2.094E-06	1.900E-06	2.426E-06	1.184E-06	1.245E-06	8.101E-07	1.577E-07	0.	0.	1.017E-05	5.574E-12
120	5.428E-07	1.564E-06	1.916E-06	2.297E-06	1.379E-06	3.028E-07	2.244E-07	0.	0.	0.	8.225E-06	3.377E-12
130	2.685E-07	7.733E-07	2.399E-06	1.212E-06	8.162E-07	1.116E-07	7.116E-09	0.	0.	C.	5.587E-06	1.884E-12
140	5.542E-07	1.502E-06	1.200E-06	1.06CE-06	1.903E-07	6.981E-08	0.	C.	0.	0.	4.577E-06	1.135E-12
150	7.914E-07	1.831E-06	6.267E-07	1.061E-06	1.110E-06	1.476E-08	0.	C.	0.	0.	5.434E-06	1.642E-12
160	2.647E-07	5.993E-07	1.221E-06	1.373E-06	2.861E-07	3.225E-10	0.	0.	0.	0.	3.743E-06	1.160E-12
170	6.932E-08	2.743E-07	1.059E-07	2.724E-07	2.276E-08	0.	0.	0.	0.	0.	7.446E-07	1.908E-13
180	2.907E-08	8.639E-08	2.432E-08	2.145E-07	9.457E-09	0.	0.	C.	0.	C.	3.638E-07	1.028E-13
SUM	4.841E-06	3.813E-05	2.018E-05	2.518E-05	1.891E-05	1.049E-04	[illegible].396E-06	8.295E-05	0.	0.	2.995E-04	3.426E-10

Table A7. Energy and Angle Distribution of the Photon Number Flux Density 30 cm above the Center of a Foxhole Exposed to 1.12-hr Fallout Consisting of the Products of one ^{235}U Fission per cm^2 of Ground Surface

(photons/cm^2-sec)

ANG/ENG	0.06	0.10	0.18	0.30	0.50	0.75	1.00	1.50	2.50	3.50	SUM	DOSE RATE
10	3.282-09	1.957-09	1.019-09	0.000+00	0.000+00	0.000+00	0.000+00	0.000+00	0.000+00	0.000+00	6.260-09	8.693-16
20	4.744-09	5.931-09	3.567-09	0.000+00	0.000+00	0.000+00	0.000+00	0.000+00	0.000+00	0.000+00	1.424-08	2.171-15
30	4.583-09	9.157-09	2.435-09	0.000+00	0.000+00	0.000+00	0.000+00	0.000+00	0.000+00	0.000+00	1.617-08	2.327-15
40	4.871-09	9.205-09	3.269-09	0.000+00	0.000+00	0.000+00	0.000+00	0.000+00	0.000+00	0.000+00	1.734-08	2.424-15
50	2.077-08	3.977-08	1.001-08	0.000+00	0.000+00	0.000+00	0.000+00	0.000+00	0.000+00	0.000+00	6.986-08	9.769-15
60	2.267-08	4.419-08	1.285-08	1.734-14	0.000+00	0.000+00	0.000+00	0.000+00	0.000+00	0.000+00	7.971-08	1.133-14
70	3.196-08	6.835-08	1.821-08	2.543-10	0.000+00	0.000+00	0.000+00	0.000+00	0.000+00	0.000+00	1.187-07	1.696-14
80	4.407-08	7.692-08	3.529-08	2.552-10	0.000+00	2.124-15	0.000+00	0.000+00	0.000+00	0.000+00	1.565-07	2.316-14
90	5.679-08	1.004-07	3.618-08	1.538-09	0.000+00	0.000+00	0.000+00	0.000+00	0.000+00	0.000+00	1.945-07	2.808-14
100	5.018-08	1.301-07	5.264-08	2.890-09	7.055-16	5.173-15	2.526-14	5.585-13	1.478-11	2.992-11	2.358-07	3.547-14
110	6.036-08	1.343-07	4.936-08	4.784-09	2.178-10	1.142-09	1.766-09	6.814-09	2.721-08	1.564-08	3.016-07	1.962-13
120	6.949-08	1.624-07	9.589-08	1.577-08	5.677-08	1.071-07	9.840-08	2.000-07	3.935-07	1.388-07	1.337-06	2.486-12
130	3.755-07	7.326-07	8.004-07	4.469-07	8.389-07	7.194-07	4.818-07	7.027-07	9.498-07	2.583-07	6.306-06	7.956-12
140	1.771-06	2.115-06	1.752-06	1.476-06	1.299-07	1.266-08	2.211-12	5.805-12	0.000+00	0.000+00	7.258-06	1.593-12
150	4.894-07	1.038-06	7.678-07	6.743-07	1.569-07	1.541-08	9.283-12	5.233-12	0.000+00	0.000+00	3.142-06	7.491-13
160	7.509-07	1.644-06	1.024-06	5.980-07	7.799-08	2.623-09	0.000+00	0.000+00	0.000+00	0.000+00	4.098-06	8.091-13
170	3.436-07	7.233-07	3.820-07	2.907-07	2.227-09	1.929-09	0.000+00	0.000+00	0.000+00	0.000+00	1.743-06	3.396-13
180	1.455-07	8.014-07	1.895-07	2.822-08	1.418-08	8.526-10	0.000+00	0.000+00	0.000+00	0.000+00	1.179-06	2.039-13
SUM	4.250-06	7.837-06	5.237-06	3.540-06	1.277-06	8.612-07	5.820-07	9.096-07	1.370-06	4.129-07	2.627-05	1.446-11

Table A8. Energy and Angle Distribution of the Photon Number Flux Density 15 cm above the Center of a Foxhole Exposed to 1.12-hr Fallout Consisting of the Products of one ^{235}U Fission per cm^2 of Ground Surface

(photons/cm^2-sec)

ANG/ENG	0.06	0.10	0.18	0.30	0.50	0.75	1.00	1.50	2.50	3.50	SUM	DOSE RATE
10	3.282-09	1.957-09	1.019-09	0.000+00	0.000+00	0.000+00	0.000+00	0.000+00	0.000+00	0.000+00	6.260-09	8.693-16
20	4.744-09	5.931-09	3.567-09	0.000+00	0.000+00	0.000+00	0.000+00	0.000+00	0.000+00	0.000+00	1.424-08	2.171-15
30	4.583-09	9.157-09	2.435-09	0.000+00	0.000+00	0.000+00	0.000+00	0.000+00	0.000+00	0.000+00	1.617-08	2.327-15
40	4.971-09	9.205-09	3.268-09	0.000+00	0.000+00	0.000+00	0.000+00	0.000+00	0.000+00	0.000+00	1.734-08	2.424-15
50	2.077-08	3.907-08	1.001-08	0.000+00	0.000+00	0.000+00	0.000+00	0.000+00	0.000+00	0.000+00	6.986-08	9.769-15
60	2.257-08	4.419-08	1.285-08	1.734-14	0.000+00	0.000+00	0.000+00	0.000+00	0.000+00	0.000+00	7.971-08	1.133-14
70	3.196-08	6.835-08	1.821-08	2.543-10	0.000+00	0.000+00	0.000+00	0.000+00	0.000+00	0.000+00	1.187-07	1.696-14
80	4.407-08	7.692-08	3.528-08	2.552-10	0.000+00	2.124-15	0.000+00	0.000+00	0.000+00	0.000+00	1.565-07	2.316-14
90	5.679-08	1.004-07	3.618-08	1.538-09	0.000+00	0.000+00	0.000+00	0.000+00	0.000+00	0.000+00	1.949-07	2.808-14
100	5.019-08	1.301-07	5.264-08	2.890-09	6.618-16	1.276-15	2.132-17	1.451-15	1.299-13	5.909-13	2.358-07	3.531-14
110	6.036-08	1.343-07	4.936-08	4.774-09	1.339-12	1.749-11	4.325-11	2.957-10	2.197-09	1.911-09	2.532-07	5.138-14
120	6.949-08	1.624-07	9.277-08	7.380-09	1.663-09	5.852-09	7.442-09	2.256-08	6.886-08	3.271-08	4.711-07	4.471-13
130	7.126-08	1.714-07	1.227-07	3.136-08	9.260-08	1.509-07	1.289-07	2.391-07	4.232-07	1.385-07	1.569-06	2.790-12
140	8.806-07	1.134-06	1.010-06	8.247-07	4.539-07	4.357-07	2.978-07	4.247-07	5.584-07	1.489-07	6.170-06	5.214-12
150	4.834-07	1.038-06	7.678-07	6.743-07	1.569-07	1.541-08	9.283-12	5.233-12	0.000+00	0.000+00	3.142-06	7.491-13
160	7.5[illegible]9-07	1.644-06	1.024-06	5.980-07	7.799-08	2.623-09	0.000+00	0.000+00	0.000+00	0.000+00	4.098-06	8.091-13
170	3.436-07	7.233-07	3.820-07	2.907-07	2.227-09	1.929-09	0.000+00	0.000+00	0.000+00	0.000+00	1.743-06	3.396-13
180	1.455-07	3.014-07	1.895-07	2.822-08	1.419-08	8.526-10	0.000+00	0.000+00	0.000+00	0.000+00	1.179-06	2.039-13
SUM	3.055-06	6.294-06	3.814-06	2.464-06	7.996-07	6.135-07	4.342-07	6.868-07	1.052-06	3.220-07	1.953-05	1.073-11

Table A9. Energy and Angle Distribution of the Photon Number Flux Density at the Center of a Foxhole Exposed to 1.12-hr Fallout Consisting of the Products of one ^{235}U Fission per cm^2 of Ground Surface

(photons/cm^2-sec)

ANG/ENG	0.06	0.10	0.18	0.30	0.50	0.75	1.00	1.50	2.50	3.50	SUM	DOSE RATE
10	3.282-09	1.957-09	1.019-09	0.000+00	0.000+00	0.000+00	0.000+00	0.000+00	0.000+00	0.000+00	6.260-09	8.693-16
20	4.744-09	5.931-09	3.567-09	0.000+00	0.000+00	0.000+00	0.000+00	0.000+00	0.000+00	0.000+00	1.424-08	2.171-15
30	4.583-09	9.157-09	2.435-09	0.000+00	0.000+00	0.000+00	0.000+00	0.000+00	0.000+00	0.000+00	1.617-08	2.327-15
40	4.871-09	9.205-09	3.268-09	0.000+00	0.000+00	0.000+00	0.000+00	0.000+00	0.000+00	0.000+00	1.734-08	2.424-15
50	2.077-08	3.907-08	1.001-08	0.000+00	0.000+00	0.000+00	0.000+00	0.000+00	0.000+00	0.000+00	6.986-08	9.769-15
60	2.267-08	4.419-08	1.285-08	1.734-14	0.000+00	0.000+00	0.000+00	0.000+00	0.000+00	0.000+00	7.971-08	1.133-14
70	3.196-08	6.835-08	1.821-08	2.543-10	0.000+00	0.000+00	0.000+00	0.000+00	0.000+00	0.000+00	1.187-07	1.696-14
80	4.407-08	7.692-08	3.528-08	2.552-10	0.000+00	2.124-15	0.000+00	0.000+00	0.000+00	0.000+00	1.565-07	2.316-14
90	5.679-08	1.004-07	3.618-08	1.538-09	0.000+00	0.000+00	0.000+00	0.000+00	0.000+00	0.000+00	1.949-07	2.808-14
100	5.018-08	1.301-07	5.264-08	2.890-09	6.618-16	1.275-15	1.906-20	3.998-18	1.207-15	1.232-14	2.358-07	3.531-14
110	6.036-08	1.343-07	4.936-08	4.774-09	3.114-14	2.860-13	1.115-12	1.351-11	1.865-10	2.450-10	2.492-07	3.829-14
120	6.949-08	1.624-07	9.276-08	7.259-09	7.665-11	3.328-10	5.840-10	2.629-09	1.235-08	7.856-09	3.557-07	[illegible].244-13
130	7.126-08	1.713-07	1.158-07	1.600-08	6.804-09	1.626-06	1.791-08	4.544-08	1.132-07	4.668-08	6.208-07	7.216-13
140	9.664-08	2.646-07	2.484-07	1.060-07	2.220-07	2.797-07	2.127-07	3.432-07	5.221-07	1.544-07	2.450-06	3.804-12
150	4.189-07	8.924-07	6.867-07	6.129-07	2.616-07	1.433-07	8.639-08	1.164-07	1.436-07	3.663-08	3.399-06	1.848-12
160	7.509-07	1.644-06	1.024-06	5.980-07	7.799-08	2.623-09	0.000+00	0.000+00	0.000+00	0.000+00	4.098-06	8.091-13
170	3.436-07	7.233-07	3.820-07	2.907-07	2.227-09	1.929-09	0.000+00	0.000+00	0.000+00	0.000+00	1.743-06	3.396-13
180	1.455-07	8.014-07	1.895-07	2.822-08	1.418-08	8.526-10	0.000+00	0.000+00	0.000+00	0.000+00	1.179-06	2.039-13
SUM	2.200-06	5.279-06	2.964-06	1.669-06	5.849-07	4.452-07	3.176-07	5.077-07	7.916-07	2.458-07	1.500-05	8.022-12

Table A10. Energy and Angle Distribution of the Photon Number Flux Density 15 cm below the Center of a Foxhole Exposed to 1.12-hr Fallout Consisting of the Products of one ^{235}U Fission per cm^2 of Ground Surface

(photons/cm^2-sec)

ANG/ENG	0.06	0.10	0.18	0.30	0.50	0.75	1.00	1.50	2.50	3.50	SUM	DOSE RATE
10	3.282-09	1.957-09	1.019-09	0.000+00	0.000+00	0.000+00	0.000+00	0.000+00	0.000+00	0.000+00	6.260-09	8.693-16
20	4.744-09	5.931-09	3.567-09	0.000+00	0.000+00	0.000+00	0.000+00	0.000+00	0.000+00	0.000+00	1.424-08	2.171-15
30	4.583-09	9.157-09	2.435-09	0.000+00	0.000+00	0.000+00	0.000+00	0.000+00	0.000+00	0.000+00	1.617-08	2.327-15
40	4.871-09	9.205-09	3.268-09	0.000+00	0.000+00	0.000+00	0.000+00	0.000+00	0.000+00	0.000+00	1.734-08	2.424-15
50	2.077-08	3.907-08	1.001-08	0.000+00	0.000+00	0.000+00	0.000+00	0.000+00	0.000+00	0.000+00	6.986-08	9.769-15
60	2.267-08	4.419-08	1.285-08	1.734-14	0.000+00	0.000+00	0.000+00	0.000+00	0.000+00	0.000+00	7.971-08	1.133-14
70	3.195-08	6.835-08	1.821-08	2.543-10	0.000+00	0.000+00	0.000+00	0.000+00	0.000+00	0.000+00	1.187-07	1.696-14
80	4.407-08	7.692-08	3.528-08	2.552-10	0.000+00	2.124-15	0.000+00	0.000+00	0.000+00	0.000+00	1.565-07	2.316-14
90	5.679-08	1.004-07	3.618-08	1.538-09	0.000+00	0.000+00	0.000+00	0.000+00	0.000+00	0.000+00	1.949-07	2.808-14
100	5.018-08	1.301-07	5.264-08	2.890-09	6.618-16	1.275-15	1.769-23	1.141-20	1.162-17	2.664-16	2.358-07	3.531-14
110	6.036-08	1.343-07	4.936-08	4.774-09	2.279-14	8.539-15	2.978-14	6.389-13	1.536-11	3.243-11	2.488-07	3.693-14
120	6.949-08	1.624-07	9.276-08	7.258-09	2.893-11	1.968-11	4.709-11	3.139-10	2.263-09	1.919-09	3.364-07	6.558-14
130	7.126-08	1.713-07	1.157-07	1.542-08	1.206-09	1.779-09	2.522-09	8.728-09	3.054-08	1.582-08	4.343-07	2.367-13
140	9.664-08	2.634-07	2.212-07	6.181-08	3.174-08	4.522-08	4.192-08	8.782-08	1.775-07	6.353-08	1.090-06	1.207-12
150	1.759-07	3.813-07	3.207-07	2.976-07	2.813-07	2.674-07	1.857-07	2.764-07	3.801-07	1.047-07	2.671-06	3.159-12
160	7.509-07	1.644-06	1.024-06	5.980-07	7.799-08	2.623-09	0.000+00	0.000+00	0.000+00	0.000+00	4.098-06	8.091-13
170	3.436-07	7.233-07	3.820-07	2.907-07	2.227-09	1.929-09	0.000+00	0.000+00	0.000+00	0.000+00	1.743-06	3.396-13
180	1.455-07	8.014-07	1.895-07	2.822-08	1.418-08	8.526-10	0.000+00	0.000+00	0.000+00	0.000+00	1.179-06	2.039-13
SUM	1.957-06	4.767-06	2.571-06	1.309-06	4.087-07	3.199-07	2.313-07	3.732-07	5.905-07	1.860-07	1.271-05	6.192-12

Table A11. Energy and Angle Distribution of the Photon Number Flux Density 30 cm below the Center of a Foxhole Exposed to 1.12-hr Fallout Consisting of the Products of one ^{235}U Fission per cm^2 of Ground Surface

(photons/cm^2-sec)

ANG/ENG	0.06	0.10	0.18	0.30	0.50	0.75	1.00	1.50	2.50	3.50	SUM	DOSE RATE
10	3.282-09	1.957-09	1.019-09	0.000+00	0.000+00	0.000+00	0.000+00	0.000+00	0.000+00	0.000+00	6.260-09	8.693-16
20	4.744-09	5.931-09	3.567-09	0.000+00	0.000+00	0.000+00	0.000+00	0.000+00	0.000+00	0.000+00	1.424-08	2.171-15
30	4.583-09	9.157-09	2.435-09	0.000+00	0.000+00	0.000+00	0.000+00	0.000+00	0.000+00	0.000+00	1.617-08	2.327-15
40	4.871-09	9.205-09	3.268-09	0.000+00	0.000+00	0.000+00	0.000+00	0.000+00	0.000+00	0.000+00	1.734-08	2.424-15
50	2.077-08	3.907-08	1.001-08	0.000+00	0.000+00	0.000+00	0.000+00	0.000+00	0.000+00	0.000+00	6.986-08	9.769-15
60	2.267-08	4.419-08	1.285-08	1.734-14	0.000+00	0.000+00	0.000+00	0.000+00	0.000+00	0.000+00	7.971-08	1.133-14
70	3.196-08	6.835-08	1.821-08	2.543-10	0.000+00	0.000+00	0.000+00	0.000+00	0.000+00	0.000+00	1.187-07	1.696-14
80	4.407-08	7.692-08	3.528-08	2.552-10	0.000+00	2.124-15	0.000+00	0.000+00	0.000+00	0.000+00	1.565-07	2.316-14
90	5.679-08	1.004-07	3.618-08	1.538-09	0.000+00	0.000+00	0.000+00	0.000+00	0.000+00	0.000+00	1.944-07	2.808-14
100	5.018-08	1.301-07	5.264-08	2.890-09	6.618-16	1.275-15	1.694-26	3.344-23	1.149-19	5.905-18	2.356-07	3.531-14
110	6.036-08	1.343-07	4.936-08	4.774-09	2.274-14	3.906-15	8.147-16	3.092-14	1.469-12	4.389-12	2.488-07	3.678-14
120	6.949-08	1.624-07	9.276-08	7.258-09	2.745-11	1.410-12	3.877-12	3.822-11	4.217-10	4.753-10	3.328-07	5.386-14
130	7.126-08	1.713-07	1.157-07	1.540-08	8.345-10	1.978-10	3.594-10	1.692-09	8.296-09	5.392-09	3.904-07	1.104-13
140	9.664-08	2.634-07	2.202-07	5.888-08	1.180-08	7.875-09	8.306-09	2.255-08	6.053-08	2.620-08	7.764-07	4.713-13
150	7.919-09	2.749-08	4.703-08	5.006-08	1.671-07	2.060-07	1.531-07	2.410-07	3.595-07	1.055-07	1.364-06	2.602-12
160	7.391-07	1.618-06	1.011-06	5.918-07	8.856-08	1.418-08	7.552-09	9.942-09	1.194-08	2.993-09	4.096-06	8.994-13
170	3.436-07	7.233-07	3.820-07	2.905-07	2.227-09	1.929-09	0.000+00	0.000+00	0.000+00	0.000+00	1.743-06	3.396-13
180	1.455-07	8.014-07	1.895-07	2.822-08	1.418-08	8.526-10	0.000+00	0.000+00	0.000+00	0.000+00	1.179-06	2.039-13
SUM	1.777-06	4.387-06	2.283-06	1.052-06	2.847-07	2.310-07	1.693-07	2.752-07	4.407-07	1.406-07	1.104-05	4.850-12

UNCLASSIFIED

Security Classification

DOCUMENT CONTROL DATA - R&D	
(Security classification of title, body of abstract and indexing annotation must be entered when the overall report is classified)	
1 ORIGINATING ACTIVITY (Corporate author) Armed Forces Radiobiology Research Institute Defense Atomic Support Agency Bethesda, Maryland 20014	2a REPORT SECURITY CLASSIFICATION UNCLASSIFIED 2b GROUP N/A
3 REPORT TITLE CALCULATED GAMMA-RAY DOSE DISTRIBUTIONS IN A PHANTOM EXPOSED TO FALLOUT AND SIMULATED FALLOUT	
4 DESCRIPTIVE NOTES (Type of report and inclusive dates) Contract Report -- Radiation Research Associates, Inc.	
5 AUTHOR(S) (Last name, first name, initial) French, R. L., Radiation Research Associates, Inc. Tompkins, K. W., Radiation Research Associates, Inc. Garrett, C. W., Armed Forces Radiobiology Research Institute	
6 REPORT DATE February 1967	7a TOTAL NO OF PAGES: 75 7b NO OF REFS: 28
8a CONTRACT OR GRANT NO DA-49-146-XZ-479 b PROJECT NO c d	9a ORIGINATOR'S REPORT NUMBER(S) AFRRI CR67-1 RRA-T71 9b OTHER REPORT NO(S) (Any other numbers that may be assigned this report)
10 AVAILABILITY/LIMITATION NOTICES Distribution of this document is unlimited.	
11 SUPPLEMENTARY NOTES	12 SPONSORING MILITARY ACTIVITY Defense Atomic Support Agency Washington, D. C. 20305

13 ABSTRACT

Gamma-ray depth-dose distributions in a phantom exposed to fallout and to simulated fallout were calculated by the Monte Carlo method. The phantom consisted of a tissue equivalent vertical right cylinder of 60 cm height and 30 cm in diameter. The center of the phantom was 3 ft 8 in. (111.8 cm) above a smooth ground surface uniformly contaminated with ^{235}U fission products. The energy and angle distribution of the gamma rays incident upon the phantom were taken from previous Monte Carlo calculations.

The depth-dose distributions were found to be relatively insensitive to fallout age over the period investigated (1 hour to 9 days). The dose rate at the center of the phantom is approximately 65 percent of the free-field dose rate, while that at the lateral surface is approximately 80 percent. Except near the extremities, the dose rate along the vertical axis of the phantom varies at approximately the same rate with height above ground as does the free-field dose rate. Approximately one-half of the dose rate at the center of the phantom is from photons which have suffered previous collisions in the phantom.

The depth-dose distributions were calculated for two arrangements of artificial sources which, although not duplicating the fallout energy spectra, were intended to produce similar depth-dose distributions. The patterns produced by revolving the phantom on its vertical axis while exposed to a point ^{60}Co source at a horizontal distance of 200 ft (61 m) are similar to those from the fallout, except for internal positions near the bottom of the phantom. A special arrangement of ^{60}Co, ^{137}Cs and ^{144}Ce sources produced substantially the same depth-dose patterns throughout the phantom as did the fallout.

An additional calculation was performed of the depth-dose distribution within a phantom positioned at the center of a 4 ft diameter by 5 ft deep foxhole located in a 1.12-hr fallout field. The distribution in the horizontal midplane of the phantom was found to be quite similar in shape to the above ground case except for a sharper dropoff of the dose away from the lateral surface. As would be expected, however, the axial distribution is quite different from that found above ground.

DD FORM 1 JAN 64 1473

UNCLASSIFIED

Security Classification

UNCLASSIFIED
Security Classification

14. KEY WORDS	LINK A ROLE	LINK A WT	LINK B ROLE	LINK B WT	LINK C ROLE	LINK C WT
fallout						
gamma rays						
depth-dose distributions						
fallout simulators						
foxholes						

INSTRUCTIONS

1. ORIGINATING ACTIVITY: Enter the name and address of the contractor, subcontractor, grantee, Department of Defense activity or other organization *(corporate author)* issuing the report.

2a. REPORT SECURITY CLASSIFICATION: Enter the overall security classification of the report. Indicate whether "Restricted Data" is included. Marking is to be in accordance with appropriate security regulations.

2b. GROUP: Automatic downgrading is specified in DoD Directive 5200.10 and Armed Forces Industrial Manual. Enter the group number. Also, when applicable, show that optional markings have been used for Group 3 and Group 4 as authorized.

3. REPORT TITLE: Enter the complete report title in all capital letters. Titles in all cases should be unclassified. If a meaningful title cannot be selected without classification, show title classification in all capitals in parenthesis immediately following the title.

4. DESCRIPTIVE NOTES: If appropriate, enter the type of report, e.g., interim, progress, summary, annual, or final. Give the inclusive dates when a specific reporting period is covered.

5. AUTHOR(S): Enter the name(s) of author(s) as shown on or in the report. Enter last name, first name, middle initial. If military, show rank and branch of service. The name of the principal author is an absolute minimum requirement.

6. REPORT DATE: Enter the date of the report as day, month, year; or month, year. If more than one date appears on the report, use date of publication.

7a. TOTAL NUMBER OF PAGES: The total page count should follow normal pagination procedures, i.e., enter the number of pages containing information.

7b. NUMBER OF REFERENCES: Enter the total number of references cited in the report.

8a. CONTRACT OR GRANT NUMBER: If appropriate, enter the applicable number of the contract or grant under which the report was written.

8b, 8c, & 8d. PROJECT NUMBER: Enter the appropriate military department identification, such as project number, subproject number, system numbers, task number, etc.

9a. ORIGINATOR'S REPORT NUMBER(S): Enter the official report number by which the document will be identified and controlled by the originating activity. This number must be unique to this report.

9b. OTHER REPORT NUMBER(S): If the report has been assigned any other report numbers *(either by the originator or by the sponsor)*, also enter this number(s).

10. AVAILABILITY/LIMITATION NOTICES: Enter any limitations on further dissemination of the report, other than those imposed by security classification, using standard statements such as:

(1) "Qualified requesters may obtain copies of this report from DDC."

(2) "Foreign announcement and dissemination of this report by DDC is not authorized."

(3) "U. S. Government agencies may obtain copies of this report directly from DDC. Other qualified DDC users shall request through ________________."

(4) "U. S. military agencies may obtain copies of this report directly from DDC. Other qualified users shall request through ________________."

(5) "All distribution of this report is controlled. Qualified DDC users shall request through ________________."

If the report has been furnished to the Office of Technical Services, Department of Commerce, for sale to the public, indicate this fact and enter the price, if known.

11. SUPPLEMENTARY NOTES: Use for additional explanatory notes.

12. SPONSORING MILITARY ACTIVITY: Enter the name of the departmental project office or laboratory sponsoring *(paying for)* the research and development. Include address.

13. ABSTRACT: Enter an abstract giving a brief and factual summary of the document indicative of the report, even though it may also appear elsewhere in the body of the technical report. If additional space is required, a continuation sheet shall be attached.

It is highly desirable that the abstract of classified reports be unclassified. Each paragraph of the abstract shall end with an indication of the military security classification of the information in the paragraph, represented as *(TS), (S), (C), or (U)*.

There is no limitation on the length of the abstract. However, the suggested length is from 150 to 225 words.

14. KEY WORDS: Key words are technically meaningful terms or short phrases that characterize a report and may be used as index entries for cataloging the report. Key words must be selected so that no security classification is required. Identifiers, such as equipment model designation, trade name, military project code name, geographic location, may be used as key words but will be followed by an indication of technical context. The assignment of links, rules, and weights is optional.

UNCLASSIFIED
Security Classification